Magnetotransport in the normal state of $La_{1.85}Sr_{0.15}Cu_{1-y}Zn_yO_4$ films

A. Malinowski and Marta Z. Cieplak
Department of Physics and Astronomy, Rutgers University, Piscataway, New Jersey 08855
and Institute of Physics, Polish Academy of Sciences, 02 668 Warsaw, Poland

S. Guha, Q. Wu, B. Kim, A. Krickser, and A. Perali
Department of Physics and Astronomy, Rutgers University, Piscataway, New Jersey 08855

K. Karpińska and M. Berkowski
Institute of Physics, Polish Academy of Sciences, 02 668 Warsaw, Poland

C. H. Shang
Department of Physics and Astronomy, The Johns Hopkins University, Baltimore, Maryland 21218

P. Lindenfeld
Department of Physics and Astronomy, Rutgers University, Piscataway, New Jersey 08855
(Received 27 August 2001; revised manuscript received 5 April 2002; published 17 September 2002)

We have studied the magnetotransport properties in the normal state for a series of $La_{1.85}Sr_{0.15}Cu_{1-y}Zn_yO_4$ films with values of y between 0 and 0.12. A variable degree of compressive or tensile strain results from the lattice mismatch between the substrate and the film, and affects the transport properties differently from the influence of the zinc impurities. In particular, the orbital magnetoresistance (OMR) varies with y but is strain-independent. The relations for the resistivity ($\rho=\rho_0+AT$) and the Hall angle ($\cot\Theta_H=\alpha T^2+C$), and the proportionality between the OMR and $\tan^2\Theta_H$ ($\Delta\rho/\rho=\zeta\tan^2\Theta_H$) are followed above about 70 K. We have been able to separate the strain and impurity effects by rewriting the last two of these relations as $\cot\Theta_H/\alpha=T^2+C/\alpha$ and $\Delta\rho/\rho=(\zeta/\alpha^2)(\alpha^2\tan^2\Theta_H)$, where each term is strain-independent and depends on y only. We also find that changes in the lattice constants give rise to approximately the same fractional changes in A, C, and α, while ρ_0 is, in addition, increased by changes in the microstructure. The OMR is more strongly suppressed by the addition of impurities than $\tan^2\Theta_H$, so that ζ decreases as y increases. We conclude that the relaxation rate that governs the Hall effect is not the same as for the magnetoresistance. We also suggest a correspondence between the transport properties and the opening of the pseudogap at a temperature which changes when the La-Sr ratio changes, but does not change with the addition of the zinc impurities. Several theoretical models seem to be in conflict with our results. Some recent ones may be more compatible, but have not been carried sufficiently far for a detailed comparison.

DOI: 10.1103/PhysRevB.66.104512 PACS number(s): 74.62.−c, 74.72.Dn, 74.76.Bz, 74.25.Fy

I. INTRODUCTION

One of the most puzzling aspects of the high-T_c superconductors is their behavior in the normal state which appears to be distinctly different from that of any other metal.[1] All normal-state properties of high-T_c superconductors display anomalous temperature dependences. In particular, their electrical charge transport is difficult to understand on the basis of a simple Drude model, in which the temperature dependence of various scattering processes is described with a single relaxation time τ. In high-T_c materials the in-plane resistivity, $\rho_{xx}\equiv\rho$, follows the relation[2,3]

$$\rho=\rho_0+AT. \tag{1}$$

The Hall coefficient $R_H=\sigma_{xy}/(H\sigma_{xx}\sigma_{yy})$ (where σ_{xx} and σ_{xy} are the longitudinal and Hall components of the conductivity tensor) is approximately proportional to $1/T$ at high temperatures,[4] while the cotangent of the Hall angle $\cot\Theta_H=\sigma_{xx}/\sigma_{xy}$ is described by the quadratic temperature dependence[5]

$$\cot\Theta_H=\alpha T^2+C, \tag{2}$$

where C is the impurity contribution.

The Drude model leads to the same T dependence for ρ and $\cot\Theta_H$, while R_H should be constant.[6] The orbital magnetoresistance (OMR) $\Delta\rho/\rho$ should vanish in materials with an isotropic Fermi surface, and be positive and proportional to τ^2 for an anisotropic Fermi surface in the weak-field regime.[6] A positive OMR has indeed been observed by Harris *et al.* for single two crystals of $YBa_2Cu_3O_{7-\delta}$ (YBCO), and for an optimally doped single crystal of $La_{1.85}Sr_{0.15}CuO_4$ (LSCO).[7] However, the OMR was found proportional to T^{-4}, and cannot be described by the same relaxation time as ρ. Instead, at high enough temperatures, the OMR follows the same T dependence as $\tan^2\Theta_H$,

$$\Delta\rho/\rho=\zeta\tan^2\Theta_H. \tag{3}$$

The relations (1), (2) have been studied in a large variety of high-T_c materials,[2,3,5,8–16] including underdoped, overdoped, and impurity-doped ones. Various deviations are found in underdoped and overdoped LSCO (Refs. 3 and 16)

and YBCO,[9,12,13] and in optimally doped and overdoped single-layer and bilayer bismuth compounds.[14,15] The relation of these deviations to the opening of a pseudogap in the normal-state excitation spectrum is still under discussion.[3,15,20,21] Conventional Fermi-liquid behavior is approached with overdoping.[3,16]

Previous measurements of the magnetoresistance are limited and do not include the influence of impurities.[7,14,17–19] In our earlier study of $La_{2-x}Sr_xCuO_4$ films with x between 0.048 and 0.275, deviations from Eq. (3) were found both in the underdoped and the overdoped regime,[19] and we suggested a link with the pseudogap opening.

The theoretical interpretation of these observations is controversial. Fermi-liquid (FL) models assume that strongly anisotropic scattering produces temperature anomalies.[9,11,22–27] Non-FL models attribute the transport behavior to the existence of two different relaxation rates at each point on the Fermi surface.[28,29] Measurements of the infrared Hall effect give support to non-FL behavior,[30] although the details do not seem to agree with any of the models. Recently, new theoretical approaches have been proposed,[31,32] motivated by angle resolved photoemission spectroscopy (ARPES) studies[33] which show that the single-particle scattering rate contains a momentum-dependent term, constant in temperature, and a momentum-independent term linear in T.

These different approaches lead to distinct predictions for the behavior of the transport parameters. A careful comparison of the predictions with the experimental data, including tests of all of the relations (1)–(3), should help to validate the models. In particular, a simultaneous study of the impurity dependence of the magnetoresistance and the Hall effect can show whether the coefficient ζ is impurity-dependent, and provide a new and sensitive test of the theories.

In this paper we present a study of the resistivity, the Hall effect, and the magnetoresistance of c-axis aligned $La_{1.85}Sr_{0.15}Cu_{1-y}Zn_yO_4$ films, with values of y, from 0 to 0.12, i.e., almost up to the composition at which the metal-insulator transition occurs at $y=0.14$.[34] In the course of this study we found that the films grow with built-in strain resulting from the lattice mismatch between the substrate and the film. The strain is relieved partially by dislocations at the interface, resulting in a variable amount of strain from film to film. Substrate-induced compressive in-plane strain is known to enhance the superconducting transition temperature,[35–37] and the origin of this effect is under discussion.[38] The compressive in-plane strain is accompanied by a decrease of the residual resistivity.[36] The influence of strain on the other transport parameters has not been previously investigated. Careful structural characterization allows us to use the variable strain in the films not only to evaluate its influence on the normal-state transport properties, but also to separate its effect out, and so to get a more precise measure of the effect of impurities.

The outline of the paper is as follows. In Sec. II we describe the experimental details. The study of the influence of strain on the structure, microstructure, and transport in LSCO films with $y=0$ (without zinc) is described in Sec. III. Section IV contains the description of the normal-state transport properties of the films with zinc. A comparison with other experiments and various theoretical models is given in Sec. V, followed by a summary in Sec. VI. Preliminary results of this study have already been described in a brief publication.[39]

II. EXPERIMENT

The specimens used in this study were c-axis aligned films grown by pulsed laser deposition on $LaSrAlO_4$ (LSAO) single-crystalline substrates.[40] The substrates were oriented with the c-axis perpendicular to the substrate surface to better then 0.2°. The growth parameters were optimized prior to this study.[40,41] During deposition the substrate was held at 720 °C in an oxygen atmosphere of 100 mTorr. The energy density of the laser pulse was held to about 1.5 J/cm^2, and the frequency to 2.1 Hz. The growth rate was about 1 Å per pulse. Particular care was taken to stabilize all growth parameters. We used computer-controlled stabilization of the laser energy, the temperature of the substrate was stabilized within 1 °C, and the oxygen flow and pressure were automatically adjusted to maintain constant values. After deposition, the oxygen pressure was increased to 750 Torr, and the films were slowly cooled to room temperature over a period of 2 h. The thicknesses of the films were in the range from 5000 to 9000 Å and we have verified that a change of thickness within this range does not influence the superconducting and transport parameters.

To separate the effects of the impurities from those of strain and microstructure, two sets of films were made. One set, with nominal composition $La_{1.85}Sr_{0.15}CuO_4$ (LSCO) and T_c between 25 and 35.2 K, was used to evaluate the correlation between the structural and the superconducting properties. In the second set of films, with nominal composition of $La_{1.85}Sr_{0.15}Cu_{1-y}Zn_yO_4$ (LSCZNO), the zinc fraction y was varied from 0 to 0.12. X-ray diffraction and absorption measurements confirmed that the value of y in the films was close to the nominal values in the targets.[41]

The specimens for the transport measurements were patterned by photolithography, and wires were attached with indium to evaporated silver pads. Simultaneous measurements of the Hall effect and the magnetoresistance were in a standard six-probe geometry in a magnetic field up to 8 T, perpendicular to the CuO_2 planes and to the current direction (transverse configuration), and for both field orientations. The magnetoresistance was also measured in the longitudinal configuration, i.e., with the magnetic field parallel to the CuO_2 planes. The temperature was varied from 25 to 300 K, and measured with a Cernox sensor, whose resistance was stabilized to about 3 parts per milllion.[19] The Hall voltage was a linear function of the magnetic field up to the highest fields used in this study.

The c-axis lattice parameters were determined from eight high-angle (00l) diffraction peaks in the θ-2θ scans measured with a Rigaku x-ray diffractometer. Both $K\alpha_1$ and $K\alpha_2$ peaks were fitted with Lorentzians, and the parameters were calculated from the least-square fits to all peak positions. The rocking curves were measured for the (008) peak. Several specimens were also studied with a four-cycle diffractometer to determine the magnitude of the a-axis lattice

parameter. The topography of the films was evaluated using Atomic Force Microscopy, with a Park Scientific Instruments AutoProbe M5.

III. LSCO FILMS: RELATION BETWEEN MICROSTRUCTURE AND TRANSPORT PROPERTIES

A. Dislocations and strain

In spite of identical growth parameters, the specimens grow with various resitivities and values of T_c, indicating the presence of disorder in the LSCO films. Similar film-to-film variations of LSCO were reported previously by other authors using reactive co-evaporation.[36] The possible origins of the disorder include strain resulting from the lattice mismatch, imperfections in the microstructure (including dislocations), and changes in the chemical composition, such as strontium or oxygen deficiency.

The in-plane lattice parameters of the film and the substrate differ by about 0.5% (the *a*-axis parameter is 3.756 Å in LSAO and 3.777 Å in LSCO), and compressive in-plane strain should therefore be expected. It has been observed in thin LSCO films,[35–37] and it has been shown that compressive strain is accompanied by *c*-axis expansion and by an increase of the superconducting transition temperature.

The degree to which the films are strained depends on the way in which the strain is relieved. If the films are very thin, of the order of several unit cells, the lattice constant may remain close to that of the substrate throughout the film. For thicker films, however, the strain is usually relieved to some degree. This may occur gradually as the distance from the substrate increases, or by dislocations right at the substrate-film interface.[42] In heteroepitaxial growth the density of dislocations is frequently the most important parameter which determines the pattern of strain relief and the microstructure of the film.[43]

In order to identify the possible causes of disorder we have made a careful study of the structure and microstructure of the LSCO films, using x-ray diffraction and atomic force microscopy (AFM). The results indicate that the variations of the transport parameters are related to the variable degree of strain present in the films, and that random disorder can be ruled out. The details of this study will be reported elsewhere.[44] In the following, we reproduce in Fig. 1 the main findings which have implications for the transport and superconducting properties.

The graph in Fig. 1 shows the correlation between the full widths at half maximum (FWHM) of the rocking curves and the *c*-axis lattice parameter for a series of films. It is seen that the films grow with various values of *c*, both larger, and smaller than the bulk. ϕ scans obtained with a four-cycle diffractometer show fourfold in-plane symmetry which persists in all specimens, indicating that the good in-plane alignment is not disturbed by disorder. We have verified that the *a*-axis parameter increases as *c* decreases, as one should expect for strain induced by lattice mismatch. The error bars on the *c* values are standard deviations from the average *c* value, calculated from eight high-angle $(00l)$ peaks. In some of the films the error bars are large, indicating a real distribution of the *c* values in these films. There is a strong correlation between the values of *c*, the distribution of *c*, and the values of FWHM. On the basis of this correlation we classify the films into four distinct types identified by different symbols in the figure.

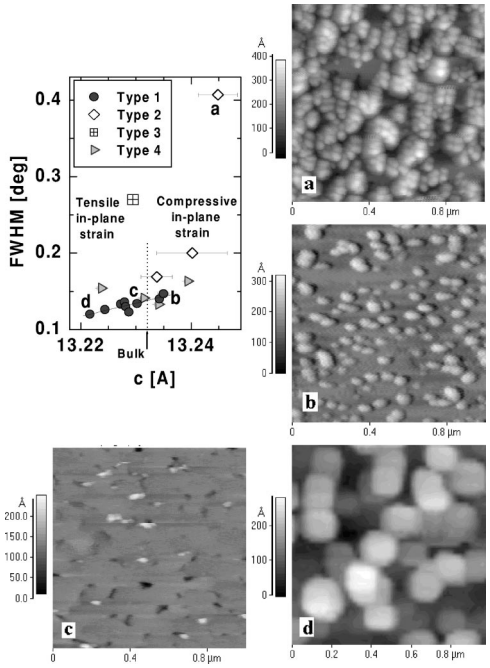

FIG. 1. FWHM as a function of *c*-axis lattice parameter for a series of $La_{1.85}Sr_{0.15}CuO_4$ films. Different symbols indicate films which belong to four groups (type 1 to type 4) as defined in the text. The bulk value of *c* is shown by the dotted line. Letters identify the films with various values of T_c and FWHM, which are shown in AFM images (a) 32 K and 0.41°, (b) 35.2 K and 0.147°, (c) 31 K and 0.134°,(d) 26 K and 0.12°.

Films of type 1 exhibit small *c*-value distributions (standard deviation less then 0.001 Å) and small FWHM (below 0.15°). These parameters indicate very good crystalline quality, uniform on the length scale probed by x rays, and we conclude that the gradual strain relief is absent in these films. Defining the strain as $\epsilon_d=(d_{\rm bulk}-d_{\rm film})/d_{\rm bulk}$ (where *d* is the lattice parameter), we observe that it ranges from about $\epsilon_a=+0.05\%$ and $\epsilon_c=-0.02\%$ (compressive in-plane strain) for the film of type 1 with the highest *c*, to about $\epsilon_a=-0.19\%$ and $\epsilon_c=+0.08\%$ (tensile in-plane strain) for the film with the lowest *c*. The FWHM decreases linearly with the decrease of *c*, indicating improvement of the crystalline quality and absence of random disorder, such as oxygen vacancies.

Films of type 2 grow with large *c* distribution (between 0.003 and 0.007 Å) and large values of FWHM (more than 0.17°, and as large as 0.41°). The correlation of these quantities suggests that the strain is relieved gradually in these films. This happens only in the films with a large average value of *c*, i.e., with large (average) compressive strain.

Occasionally films grow as type 3 (only one such film is shown in Fig. 1), with a large value of FWHM, but without a large *c* distribution. The gradual strain relief is absent. The large FWHM is presumably the result of some other disorder.

Finally, a substantial number of films, classified as type 4, show a borderline behavior between films of type 1 and type 2, that is, either FWHM, or the c distribution, or both, are somewhat enhanced in comparison with type 1 films, but they are still substantially smaller than in type 2 films. It is reasonable to assume that the regions with gradual strain relief may coexist in these films with strained regions. We refer to this type of film as ''mixed.''

A direct look at the microstructure of the films can be obtained with AFM [images (a) to (d) in Fig. 1]. We find that the films with gradual strain relief grow with grains of various sizes, from about 50 nm to 200–500 nm [image (a)], characteristic for three-dimensional (3D) growth. The root-mean-square (r.m.s.) roughness is as large as 7 nm in these films. Similar microstructure, indicative of 3D growth, is observed also in films of type 3. This explains the large values of FWHM observed in these films.

The grains in the films of type 1, without gradual strain relief, are more uniform in size [images (b) to (d)]. The cross sections of the images indicate that the films start as islands, several unit cells high at a time. In the films with small compressive or tensile strain these islands coalesce into quite smooth surfaces, with r.m.s. roughness of the order of one to two unit cells. The images (b) and (c) represent this regime, with the difference between them resulting from different times at which the growth terminates. We refer to this type of growth as ''quasi 2D.''

The microstructure of the films of type 1 evolves further when the strain becomes more and more tensile. We observe that substantial imperfections appear at the grain boundaries when the grains coalesce. In the film with the lowest c we observe the formation of very flat, imperfectly connected grains [image (d)]. The grains are quite uniform in size, about 150 nm across, with very good crystalline quality inside the grains. The r.m.s. roughness increases again, to about 6 nm.

AFM images of the films of type 4 indicate that in most of them the growth is close to quasi-2D, but with occasional admixture of 3D areas. This confirms the ''mixed'' character of these films.

We interpret the evolution of the microstructure as resulting from the different amount of dislocations created at the substrate-film interface. In films with negligible strain a small number of dislocations nucleated at the interface relieves the strain fully, allowing for the formation of a quasi-2D film with the lattice parameters very close to the bulk values. As the number of dislocations at the interface decreases, the films should grow with larger built-in compressive in-plane strain. However, this type of growth is unstable in thick films. Only occasionally do thick films grow with uniform compressive strain, and this occurs only for strain smaller then about 0.023%. Larger compressive strain is usually relieved gradually. This contributes to the deterioration of growth to the 3D type.

When the number of dislocations at the interface increases, the films grow with built-in tensile strain. This type of growth is more stable than the growth with compressive strain, since any additional disorder may be more easily accommodated in the vicinity of more numerous dislocations. As a result, the quasi-2D growth occurs for larger tensile strains (up to 0.08%), and the FWHM decreases as the tensile strain grows. However, as the density of dislocations increases, they may have a tendency to cluster.[43] Presumably this is the origin of the formation of imperfectly connected grains in films with large tensile strain [as in image (d) in Fig. 1].

This picture provides a consistent explanation for the evolution of the microstructure of the films with the built-in strain. Film-to-film variations are observed also for LSCO films grown by reactive coevaporation.[36] It is very likely that the existence of dislocations is common to different growth methods. Note that the control of the density of dislocations in heteroepitaxial growth is a very difficult problem. In the well-known semiconducting technologies elaborate procedures were invented to clean the substrate and the growth chambers in order to reduce the density of dislocations.[43] The process of growth of perovskite oxides proceeds in an oxygen atmosphere, and so far little is known about the influence of these conditions on the substrate-film interface.

B. Resistivity and Hall effect

The films with gradual strain relief are not suitable for the studies of the intrinsic properties of LSCO. Therefore, in the following we will restrict the discussion mainly to films of type 1. In addition, we will include some films of type 4. In these films the c-distribution and FWHM are only slightly enhanced in comparison with films of type 1, but we will show that some of the normal-state properties are considerably modified in them.

Figure 2(a) shows several typical examples of the temperature dependence of the resistivity. The data are labeled with the value of the $T=0$ intercept of the resistivity, ρ_0, determined from the fit of Eq. (1) between 200 and 300 K. In the following we will refer to the parameter ρ_0 as the ''residual resistivity,'' as is frequently done by others.[5,45,46] It is not the same as the residual resistivity defined in conventional metals, but it resembles the residual resistivity in many respects. For example, impurities introduce an additive term to ρ_0.

In Fig. 2(a) the three curves with lower values of ρ_0 are for films of type 1, and the two curves with larger values are for films of type 4. This pattern of larger ρ_0 in films of type 4 persists for most of them. Interestingly, the slope of the T dependence of the resistivity A does not grow as fast as the residual resistivity. This is shown in the inset in Fig. 1(b), where we include the data from a larger set of LSCO films. While ρ_0 increases by a factor of about 7 in this set, A increases by a factor of at most 2.

Figure 3 shows the cotangent of the Hall angle measured in a magnetic field of 8 T as a function of T^2 for the same set of films as in Fig. 2(a). It is seen that the data follow straight lines except at the lowest temperatures. The values of the intercept c and the slope α of the Hall-angle lines from the fit to Eq. 2 are shown in the inset to Fig. 3(b). Remarkably, C is proportional to α, in contrast to the relation between ρ_0 and A shown in Fig. 2(a). The proportionality between C and α is

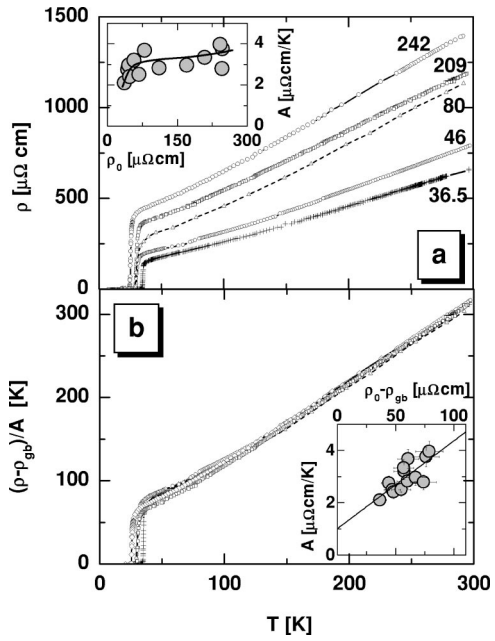

FIG. 2. (a) The temperature dependence of the resistivity for several $La_{1.85}Sr_{0.15}CuO_4$ films. The data are labeled with the value of ρ_0 for each film (in $\mu\Omega$ cm). (b) $(\rho-\rho_{gb})/A$ as a function of T for the same set of samples as in (a). ρ_{gb} is the grain boundary resistivity, as defined in the text. Inset: $\rho_0-\rho_{gb}$ as a function of A for a larger set of films. The line is fitted to the data.

also illustrated in Fig. 3(b) which shows $\cot\Theta_H$ divided by α. It is seen that the data for films with different values of ρ_0 collapse to a single line.

Figure 2(a) shows that the increase of ρ_0 is accompanied by a decrease of T_c, from 35.2 K in the film with the highest, to 25 K in the film with the lowest T_c. The decrease of

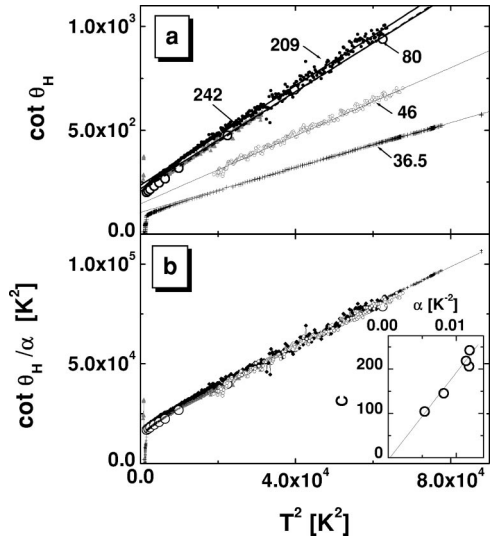

FIG. 3. (a) $\cot\Theta_H$ at 8 T as a function of T^2 for the same films as in Fig. 1(a). The lines are fits to the relation $\cot\Theta_H=\alpha T^2+C$, and the data are labeled with the value of ρ_0. (b) $\cot\Theta_H/\alpha$ as a function of T^2: the data collapse to one line. Inset: C vs α for the same set of films.

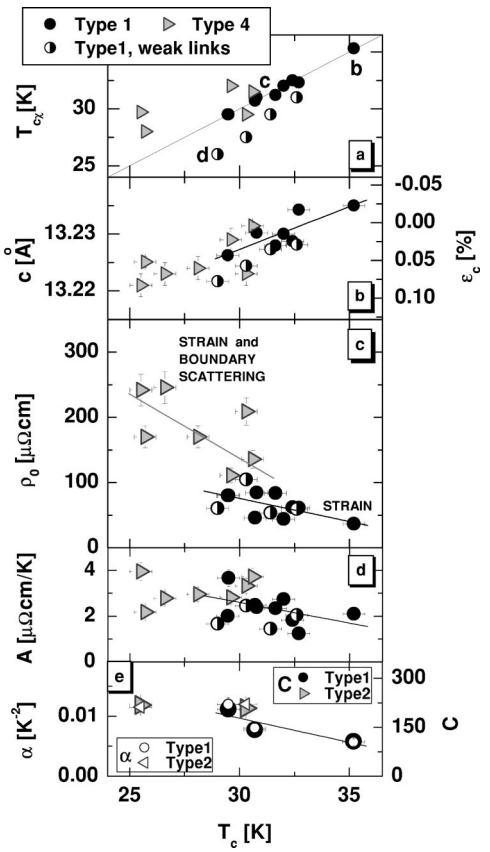

FIG. 4. The correlation between the resistive superconducting transition temperature T_c and several other parameters: (a) the magnetically determined $T_{c\chi}$, (b) c, (c) ρ_0, (d) A, (e) C (closed symbols) and α (open symbols). Films are divided into three groups marked by different symbols: type 1 (closed circles), type 1 with weak links (half-filled circles), and type 4 (triangles). The letters in (a) identify the films which are shown in the AFM images of Fig. 1. All lines are linear fits to the data for type 1 films.

T_c occurs in films of both types, 1 and 4. A detailed examination of the superconducting transitions, which will be presented elsewhere,[44] shows that the lowering of T_c is associated with a substantial broadening of the transition. However, the broadening has a different character for films of type 1 and type 4. It is convenient to describe this effect by comparing the resistive transition temperature T_c defined as the midpoint of the resistive transition, and the magnetically determined transition temperature $T_{c\chi}$. This comparison is shown in Fig. 4(a). In good quality films we expect T_c to be very close to $T_{c\chi}$ so that the data points should follow the straight line drawn in the figure. The data for the majority of films of type 1 indeed follow this line, including the data for films marked (b) and (c), for which AFM images show smooth surfaces in Fig. 1. However, in films with large tensile strain, such as film (d), imperfectly connected grains appear. Imperfectly connected grains create weak links at the grain boundaries, and cause the behavior characteristic for granular superconductors.[48] When the temperature is lowered, two distinct transitions are observed, one when the inside of the grains becomes superconducting at T_c and the other when bulk superconductivity occurs at the lower (mag-

netically measured) temperature $T_{c\chi}$. In these films $T_{c\chi}$ is lower than T_c. The films in which weak links are observed are marked by half-filled symbols in Fig. 4.

Some of the films of type 4 show the opposite effect, i.e., $T_{c\chi}$ is higher then T_c. This may happen when the films contain some areas with 3D growth and gradual strain relief. Usually in this type of film the layer closest to the substrate is most strained, and the superconductivity occurs there, as detected by $T_{c\chi}$. However, in the 3D areas the current flows along percolating paths, which may meander away from the most strained layer. Hence the resistive transition may occur at a lower temperature.

Figure 4(b) shows the relation between T_c and the *c* axis lattice parameter. The magnitude of the strain ϵ_c is shown on the right-hand scale. Note that specimens with the same average strain may show quite different values of T_c, depending on the microstructure of the film. The straight line fitted to the data for films of type 1 (excluding the films with weak links) gives the rate of decrease of T_c with *c* equal to 670 K/Å. This value is more than three times as large as the rate reported by Sato *et al.*[36] for LSCO films with $0.12<x<0.18$. It is possible that a variation in the amount of strontium affects the rate, or that the microstructure of the films prepared by reactive coevaporation[36] is different from that of films grown by pulsed laser deposition, so that a straightforward comparison of the results is difficult.

In the films of type 1 without weak links the strain ranges from about $\epsilon_a=+0.05\%$ and $\epsilon_c=-0.02\%$ (compressive in-plane strain) for the film with the highest T_c, to about $\epsilon_a=-0.13\%$ and $\epsilon_c=+0.05\%$ (tensile in-plane strain) for the film with the lowest T_c. The change of T_c induced by the compressive or tensile strain may be found from the expression[37] $T_c=T_c(0)+2(\delta T_c/\delta\epsilon_{ab})\epsilon_{ab}+(\delta T_c/\delta\epsilon_c)\epsilon_c$, where $\delta T_c/\delta\epsilon_i$ ($i=a,b$, or *c*) are the uniaxial strain coefficients. The values of the coefficients were estimated in Ref. 47, as $\delta T_c/\delta\epsilon_a=(250\pm340)$ K, $\delta T_c/\delta\epsilon_b=(400\pm340)$ K, and $\delta T_c/\delta\epsilon_c=(-1090\pm1120)$ K. Using the average of the values for the *a* and *b* axes as 325 K, and for the *c* axis as -1090 K, we estimate that compressive and tensile strain should change T_c by about $+1$ and -1.4 K, respectively, so that the maximum change of T_c directly related to strain should not exceed 2.5 K. The experiment shows a change of about 6 K. With the large uncertainty of the strain coefficients the agreement is reasonable.

The correlation between T_c and the transport parameters ρ_0, *A*, *C*, and α for the LSCO films is summarized in Figs. 4(c) to 4(e). We see that as T_c decreases, all of these parameters increase. The black lines show linear fits to the data for films of type 1 without weak links. The fractional changes of ρ_0, *A*, *C*, and α are approximately the same for these films, about $(15\pm5)\%$ per K. Note that there appears to be no difference between films with and without weak links, so that in contrast to the effect on T_c, the grain boundaries in films of type 1 have negligible effect on the transport properties in the normal state. This suggests that the increase of the transport parameters in films of type 1 is an effect caused by the strain alone.

A, *C*, and α follow the same dependence, with approximately the same fractional changes, in films of type 4. On the other hand, ρ_0 is enhanced in these films with values of ρ_0 reaching more then 100 $\mu\Omega$ cm. Since the magnitude of the strain is similar in films of type 1 and type 4, it follows that the enhancement must be caused by effects other than strain. A conceivable origin of the enhancement is a change of chemical composition such as a deficiency of strontium or oxygen, which could create scattering centers and decrease the carrier concentration. However, this cannot be the sole cause of the observed effects. A decrease in carrier concentration is known to lead to a decrease of the slope of the cotangent line,[16,19] contrary to the result shown in Fig. 4(e). We conclude that the film morphology must be responsible. The mixed films contain some areas with 3D growth. The grain boundaries in these areas are more disordered and numerous then the grain boundaries in films of type 1, and so they cause substantial grain boundary scattering. Accordingly, we mark in Fig. 4(c) two regimes: the regime of ''strain'' in films of type 1, and the regime of ''strain and boundary scattering'' in films of type 4.

The fact that *A*, *C*, α, and in the films of type 1 also ρ_0, undergo the same fractional changes, suggests that the strain affects all transport coefficients in the same way, while grain-boundary scattering affects only the residual resistivity in films of type 4, introducing an additive contribution to ρ_0, which we call ρ_{gb}. If this is indeed the case, then the quantity $\rho_0-\rho_{gb}$ should depend on strain only, and therefore should be proportional to *A*. To estimate this quantity in type 4 films, we first extrapolate the linear relation between ρ_0 and T_c from the dependence for films of type 1, where $\rho_{gb}=0$, as shown by the black line in Fig. 4(c), and calculate the value of $\rho_0-\rho_{gb}$ for each sample from its value of T_c. The inset to Fig. 2(b) shows that the calculated $\rho_0-\rho_{gb}$ is indeed closely proportional to *A*. The temperature dependence of $\rho-\rho_{gb}$ divided by *A* is shown in the main part of Fig. 2(b) for the same set of films as displayed in Fig. 2(a). We see that the data for different films collapse on the same line, with small deviations appearing only below 100 K, probably because of imperfect estimates of ρ_{gb}. This result confirms the consistency of our analysis and shows that the conclusions about the distinct effects of strain and grain–boundary scattering in the films of different types are correct.

IV. LSCZNO FILMS: IMPURITIES AND STRAIN

A. Resistivity

We now turn to the specimens in which zinc is substituted for some of the copper. The temperature dependence of the resistivity for some of these films (normalized to the value at room temperature $\rho_{295\,\mathrm{K}}$), is shown in Fig. 5. This set of films was selected for small ρ_0, and it is shown here to emphasize the evolution of the temperature dependence on doping. However, in all films the resistivity is dependent on both the impurities and the strain, and we discuss these dependences in more detail below. The inset shows the dependence of $\rho_{295\,\mathrm{K}}$ on *y*. These values are about 30% higher than in similar single crystals.[46] However, while in the single

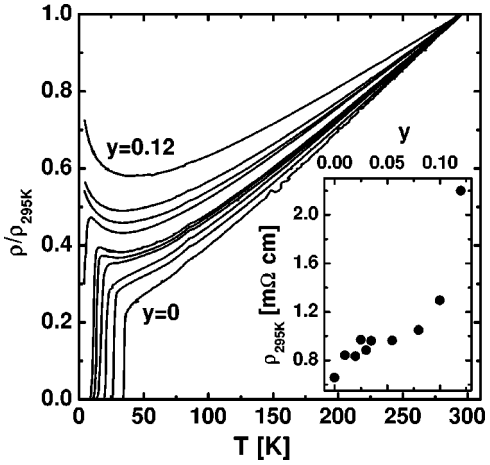

FIG. 5. Temperature dependence of the resistivity (normalized to room temperature) of a series of $La_{1.85}Sr_{0.15}Cu_{1-y}Zn_yO_4$ films with $y=0,0.01,0.02,0.025,0.03,0.035,0.055,0.08,0.10,0.12$ (from bottom to top). Inset: the room-temperature resistivity as a function of y.

crystals zinc can be added only up to $y=0.04$, three times as much can be added in the films. The room-temperature resistivity increases linearly with y up to about $y=0.1$. For larger y the increase is faster than linear as a result of the approach to the metal-insulator transition, as described in a previous publication.[34] The films remain superconducting up to $y=0.055$, and the films with $0.055<y<0.12$ are metallic but nonsuperconducting. In the ceramic specimens superconductivity dissapears for $y=0.03$.[49]

In all films the resistivity is linear in T at high temperatures. We fit the high-T resistivity between 200 and 300 K with Eq. (1) to obtain ρ_0. Just as in the case of undoped LSCO, the films grow with various values of T_c and residual resistivity for any given value of y. The correlation between T_c and ρ_0 for films with zinc was already discussed in Refs. 34 and 41, where we found that for films with small ρ_0 the dependence of T_c on ρ_0 is well described by the Abrikosov-Gorkov formula.[50] In Fig. 6 we show ρ_0 as a function of T_c. We include the data for $y=0$ of Fig. 4(c) as well as the fit to

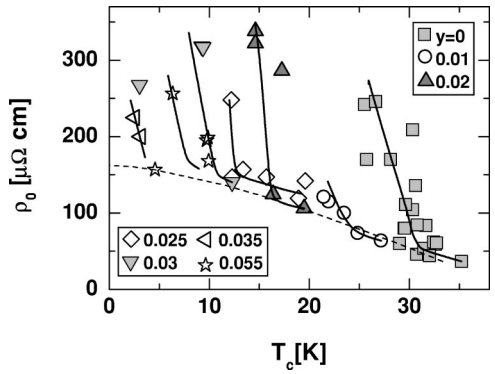

FIG. 6. The residual resistivity ρ_0 as a function of T_c for films with various values of y. The dashed line is drawn through the data for films with $\rho_s<100\ \mu\Omega$ cm, which follow the Abrikosov-Gorkov formula. All other lines are guides to the eye.

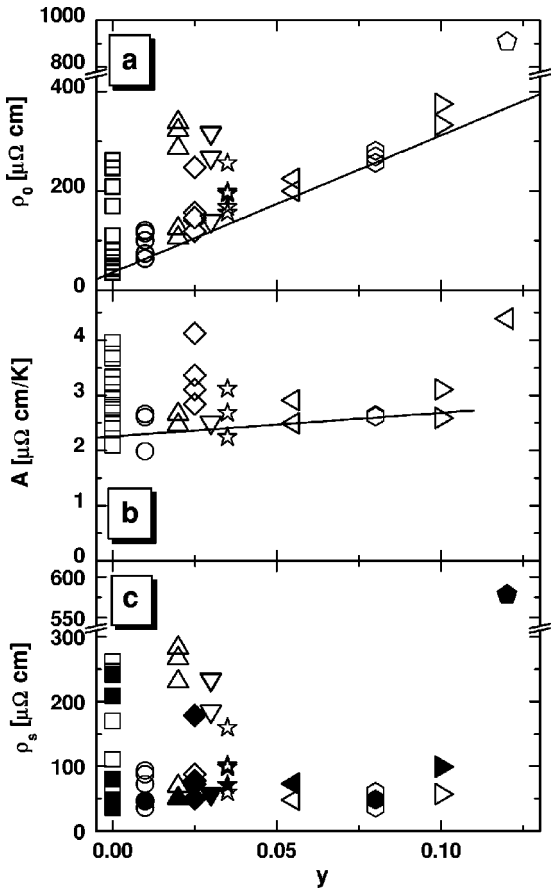

FIG. 7. The residual resistivity ρ_0 (a), the resistivity slope A (b), and strain-related residual resistivity, ρ_s (c), as a function of y. The black points in (c) indicate films for which the Hall effect was measured.

the Abrikosov-Gorkov formula from Ref. 34. Data for $y=0$ show a crossover in the ρ_0-vs-T_c line around T_c equal to 30 K, which results from two distinct dependences of $\rho_0(T_c)$ in films of type 1 and type 4. We see that a similar crossover is also present for other values of y, so that we expect our interpretation of strain, dislocations, and grain boundary scattering to be the same in the films with zinc as in those without.

We now proceed to the separation of the effects of strain and grain-boundary scattering from the effect of the zinc impurities. On Fig. 7(a) we show the dependence of ρ_0 on y, for all the films with various values of the residual resistivity for each value of y. We see that the minimum value of ρ_0 increases linearly with increasing y. We assume that this minimum value is the residual resistivity associated with the zinc impurities, and call it ρ_y. The rate of increase of ρ_y with y is $\rho_y/y=2.8$ mΩ cm. This value is comparable to the rate observed in single crystals of YBCO with zinc.[5] (Because of its closeness to the metal-insulator transition we have excluded the film with $y=0.12$ in the analysis.)

The slope A is shown as a function of y in Fig. 7(b). In contrast to ρ_0 it does not change dramatically with y. In fact, if we fit a straight line to the data for the films with the minimum residual resistivity for each y (again excluding $y=0.12$), we find that A changes by about 17% as y changes

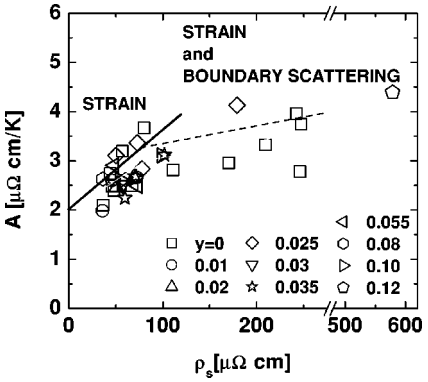

FIG. 8. A as a function of ρ_s for films with different values of y. The solid line is a linear fit in the strain regime and the dashed line is a fit for films with grain-boundary scattering, with ρ_s larger than about 100 $\mu\Omega$ cm.

from zero to $y=0.1$, not far from the experimental error of about $\pm 10\%$. The same conclusion of a very weak influence of zinc impurities on A may be reached from data for single crystals of YBCO and LSCO,[46] although an earlier report noted a substantial increase of A.[5] The variability of the results may be related to differences in the microstructure of the specimens rather than to a change of A with y. In any case, we conclude that A remains almost unchanged by the addition of the impurities.

If ρ_y is the zinc-related part of the residual resistivity, then the difference $\rho_s=\rho_0-\rho_y$ is the part which results from strain and grain-boundary scattering. Its dependence on y is shown on Fig. 7(c), where we see that its minimum value does not depend on y.

The separation into a y-dependent and a y-independent part shows that Matthiessen's rule is valid and that we can have confidence in the relation

$$\rho_0=\rho_y+\rho_s\,. \tag{4}$$

We can test this relation further by investigating the relation of ρ_s to the other transport parameters. The relation of A to ρ_s is shown on Fig. 8. In spite of considerable scatter we can identify two different regimes. When ρ_s is smaller than about 100 $\mu\Omega$ cm, A increases rapidly, while for larger ρ_s a crossover is seen to a much weaker increase. This crossover is similar to that of Fig. 4(c), i.e., it is caused by more rapid increase of ρ_s in the grain-boundary scattering regime. We will see that a similar conclusion can be drawn from the Hall-effect data.

B. Hall effect

On Fig. 7(c) we show by black points the specimens for which the Hall effect was studied. The influence of strain on the Hall angle was already discussed for $y=0$. To see how the zinc impurities change the strain-related effects, we have measured several films with $y=0.025$ and with different values of ρ_s, including the film with $\rho_s>100$ $\mu\Omega$ cm, in the grain-boundary scattering regime. The transport parameters for the films in which the Hall effect was studied are collected in Table I. The table also includes the data on magnetoresistance which will be discussed in the next section.

TABLE I. Transport parameters of the films of $La_{1.85}Sr_{0.15}Cu_{1-y}Zn_yO_4$. The definitions of all parameters are given in the text. The experimental accuracy is about ± 15 the last column, and about ± 10

y	ρ_0 ($\mu\Omega$ cm)	T_c (K)	A $\left(\frac{\mu\Omega\,\mathrm{cm}}{\mathrm{K}}\right)$	α 10^{-3} K^{-2}	C	$\zeta\left(\frac{\alpha_0}{\alpha}\right)^2$
0	36.5	35.2	2.10	5.65	106	11.05
0	46.0	30.7	2.49	8.00	142	
0	80.0	29.5	3.67	11.9	206	11.15
0	209	30.3	3.33	12.0	242	
0	242	25.5	3.96	11.7	218	
0.01	73.8	26.5	2.60	7.52	150	10.6
0.02	106	21.0	2.46	7.81	166	8.00
0.025	119	20.4	3.11	8.22	194	7.21
0.025	147	17.1	2.84	8.85	220	7.66
0.025	248	13.5	4.13	13.7	340	7.01
0.03	140	13.6	2.51	7.47	195	6.04
0.035	168	11.5	2.68	8.35	228	6.52
0.055	225	3.6	3.11	10.1	323	5.11
0.08	269	0	2.64	8.00	313	3.28
0.10	375	0	3.11	14.6	652	3.78
0.12	910	0	4.39	21.4	1090	

On Fig. 9 we show the temperature dependence of the Hall coefficient for selected films with various values of y. We see that the zinc causes a decrease of R_H without appreciably affecting the shape of $R_H(T)$. This behavior is quite different from that observed in LSCO when the strontium-lanthanum ratio is changed, both in the underdoped and in the overdoped regimes.[16,19] With decreasing strontium the metal-insulator transition is approached as a result of the decrease in the carrier concentration. This leads to an increase of the Hall coefficient by a factor of about 6.[19] In the films with zinc, on the other hand, the decrease of R_H is quite

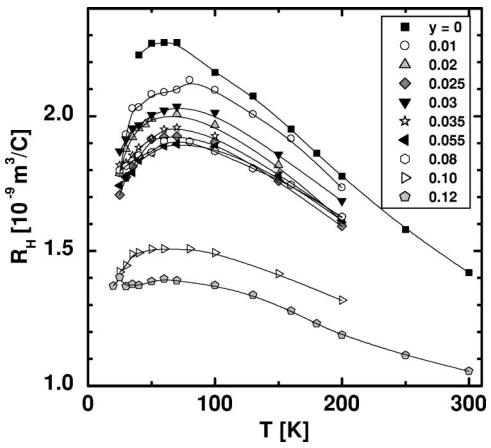

FIG. 9. Temperature dependence of the Hall coefficient R_H for a series of films with various values of y.

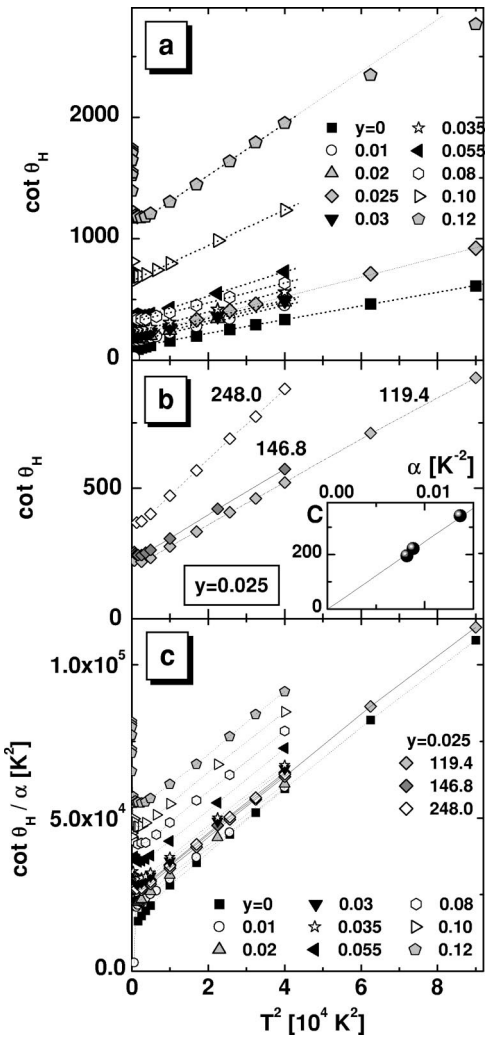

FIG. 10. (a) and (b) cot Θ_H at 8 T, (c) cot Θ_H/α as a function of T^2. The lines are fits to the equation cot $\Theta_H = \alpha T^2 + C$. In (a) the data are for films with different values of y; in (b) the data are for $y = 0.025$ and different values of ρ_0 (in $\mu\Omega$ cm); in (c) all the data are included. The solid lines are drawn through the data for the films with $y = 0.025$. Inset in (b): the correlation between C and α for films with different values of ρ_0.

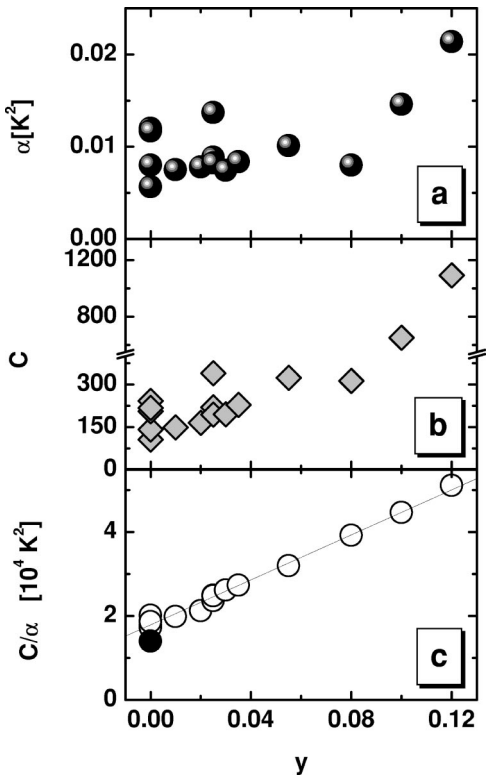

FIG. 11. α (a), C (b), and C/α (c) as a function of y. The full point in (c) is for the $La_{1.83}Sr_{0.17}CuO_4$ single crystal of Harris *et al.*, Ref. 8.

modest, only by a factor of about 1.6. This underscores the fact that with the addition of zinc the metal-insulator transition is quite different, driven by disorder, rather than by a change in the carrier concentration.[34]

The influence of the zinc on the cotangent of the Hall angle is shown in Fig. 10. Part (a) shows the data as a function of T^2 for films with different y. A few of the specimens were measured to 300 K, the rest to 200 K. It is seen that the data for most of the films follow straight lines, except for upturns below about 70 K in the films with $y > 0$. The upturns may be related to localization effects, or to the opening of a pseudogap. There is also a small deviation from the straight line in the film with $y = 0.12$ for $T > 200$ K, presumably because of the vicinity of the metal-insulator transition. Apart from these deviations, Eq. (2) is followed, even in films with so much zinc that there is no longer any superconductivity. This is quite different from the behavior observed when the strontium content is altered in LSCO, when deviations are observed away from optimal doping, particularly in the overdoped region.[16,19]

An increase of zinc causes an increase in the cotangent of the Hall angle. However, the lines do not progress monotonically with y. For example, the line for $y = 0.08$ is below that for $y = 0.055$. The reason is the random variation of strain from film to film. This can best be seen on Fig. 10(b), where we show data for three films with $y = 0.025$ and different values of the residual resistivity. The inset shows that c and α are again proportional to each other. Just as before for $y = 0$ (Fig. 3), the three lines collapse to one if instead of cot Θ_H we plot cot Θ_H/α [Fig. 10(c)]. Moreover, on this graph the increase of cotΘ_H/α with increasing y is monotonic.

This is also illustrated on Fig. 11, where the two top panels show α and c as functions of y for all films, including the three films with $y = 0.025$ and the five films with $y = 0$ from Fig. 3. The scatter of the parameters disappears when we plot the ratio C/α [Fig. 11(c)]. The strain affects both parameters in the same way, so that C/α is a function of y only. We see further that C/α increases linearly with increasing y.

Figure 12(a) shows the dependence of α on ρ_s for all films measured in this study. For ρ_s less than 100 $\mu\Omega$ cm the points fall on a straight line, regardless of the value of y. For larger ρ_s there is a crossover to a different regime. This is the same behavior as that of A shown on Fig. 8. It follows that α is y independent, and depends on strain in a similar fashion for all films regardless of y. The relation between α and ρ_s is

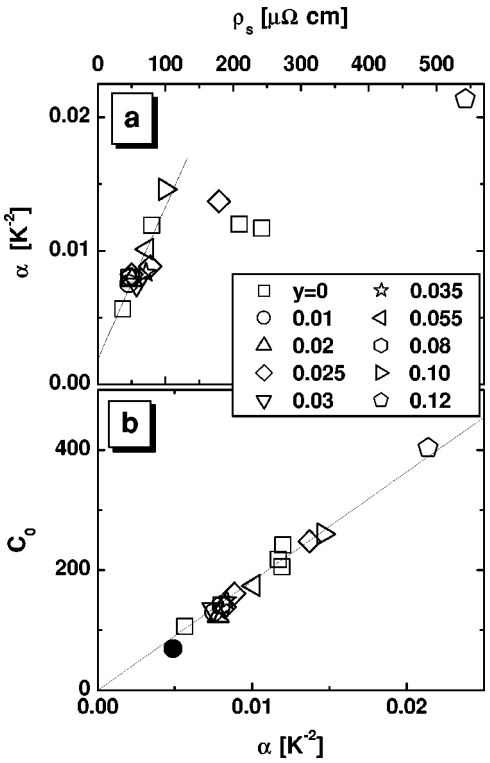

FIG. 12. (a) α as a function of ρ_s for films with different values of y. The line is a linear fit in the regime of small ρ_s, i.e., without grain-boundary scattering. (b) The proportionality between C_0 and α. The full point is for the $La_{1.83}Sr_{0.17}CuO_4$ single crystal of Harris *et al.*, Ref. 8.

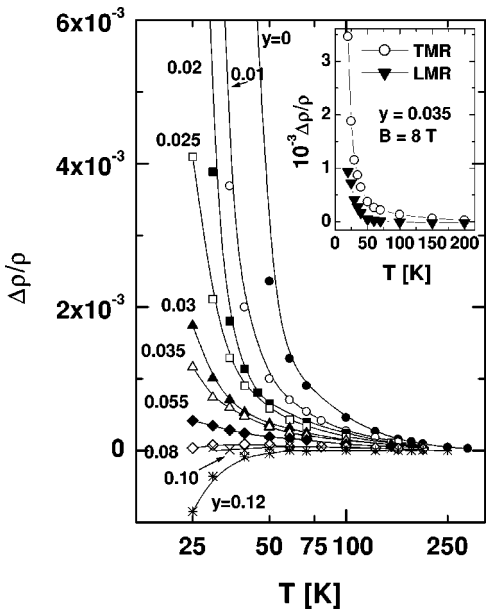

FIG. 13. The orbital magnetoresistance at 8 T as a function of $\ln T$ for a series of films with various values of y. Inset: The TMR and the LMR as a function of temperature for the film with $y = 0.035$.

also a further indication that the separation of ρ_0 into ρ_y and ρ_s is correct. A previous study of YBCO crystals with zinc[5] without strain finds α also to be y independent, and equal to 5.11×10^{-3} K^{-2}, close to the minimum in our films.

Since α is y independent, and C/α depends on y only, we conclude that C is a linear function of y: $C=C_0+C_1y$. The fit to the data in Fig. 11(c) gives two parameters: $C_0/\alpha = (1.8\pm0.1)\times10^4$ K^2 and $C_1/\alpha=(2.6\pm0.2)\times10^5$ K^2.

We summarize the behavior of the Hall angle by rewriting Eq. (2) as

$$\cot\Theta_H/\alpha = T^2 + C/\alpha, \tag{5}$$

$$C = C_0 + C_1 y, \tag{6}$$

where each term in Eq. (5) is strain independent and a function of y only. α and C depend on strain in the same way, and α is y independent. Fig. 12(b) shows C_0 as a function of α for all films. The data lie closely on a straight line, including even the specimen with $y=0.12$, close to the metal–insulator transition, as well as the point for the single crystal of LSCO.[7]

C. Magnetoresistance

The magnetoresistance measurements were performed in two configurations of the magnetic field with respect to the CuO_2 planes. In nonsuperconducting films, i.e., for $y > 0.055$, both the longitudinal and the transverse magnetoresistance (LMR and TMR, respectively) are negative at very low temperatures, with increasing magnitude as y increases. The analysis of this effect, to be presented elsewhere,[51] suggests that it originates in the spin-disorder scattering of carriers on magnetically ordered spin droplets around Zn impurities.

In this paper we concentrate on the regime of high temperatures, from 25 to 300 K. The inset to Fig. 13 shows the T dependences of the LMR and the TMR for a film with $y = 0.035$. The TMR is positive over the whole temperature range, for all values of y, and decreases with increasing y. The LMR has a more complicated behavior, but it is always smaller than the TMR, by a factor of 3 to 10, approaching the experimental resolution of the measurements at high temperature. At the highest temperatures the LMR is slightly negative and becomes positive as T is lowered below about 50 to 150 K. We attribute the LMR to isotropic spin scattering. Spin scattering may be expected to grow with increasing y since zinc-doping produces enhanced staggered magnetization around impurity sites.[52] Subtracting the LMR from the TMR we obtain the orbital magnetoresistance (OMR), which is shown in the main part of Fig. 13 for a series of films with various values of y.

The OMR is positive in most of the films, but decreases rapidly with increasing y until, in the film closest to the metal-insulator transition ($y=0.12$), it becomes negative below about 50 K. In fact, we can see in Fig. 5 that the resistivity of this film shows an upturn in the vicinity of 50 K. Presumably the negative OMR is related to the localization effects which dominate the behavior close to the metal-insulator transition.

In Fig. 14 we show the T dependence of the OMR on a double logarithmic plot for the films with positive OMR. There are two important features in this graph. First, the

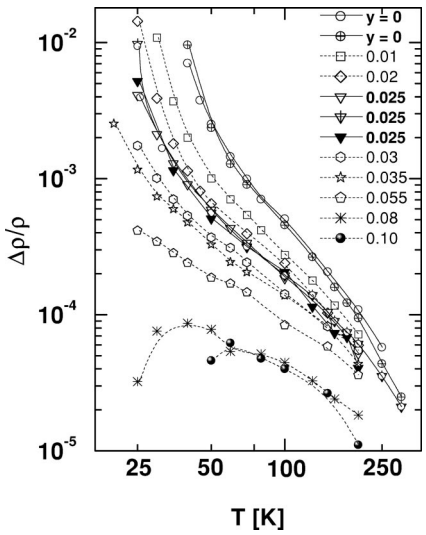

FIG. 14. Log-log plot of the orbital magnetoresistance at 8 T as a function of temperature for a series of films with various values of y. All lines are guides to the eye. The solid lines are drawn through the data for $y=0$ and $y=0.025$, for which several films with different ρ_0 were measured.

magnitude of the OMR decreases monotonically with increasing y. This suggests that the OMR is not sensitive to strain effects. This is confirmed by the lines for $y=0$ and for $y=0.025$, which include data for several films with different residual resistivities. They can be seen to be following closely along single lines for each value of y, showing that the OMR is not influenced by strain but depends solely on y.

The second interesting feature is the shape of the OMR curves. The lines for all superconducting specimens ($y>0.055$) have a characteristic ''S shape,'' as previously observed in optimally doped LSCO and YBCO.[7,19] The high-temperature part of the data, from about 70 to 300 K, is convex and as discussed in Refs. 7 and 19 follows the T dependence of the square of the Hall angle in accord with Eq. (3). At lower temperatures, below about 70 K, the lines deviate upwards. The deviation leads to an inflection point which gives the curves their S shape.

We have noted previously[19] that the inflection point moves to higher temperatures when the strontium fraction is decreased, until in strongly underdoped LSCO the curves lose their S shape, as the region of validity of Eq. (3) moves to higher temperatures, beyond the region of the measurements. In contrast, we see that the zinc impurities do not affect the shape of the curves. They retain their S shape, at least in all superconducting specimens, showing that Eq. (3) remains valid for all films above 70 K. We have suggested previously that the position of the inflection point is related to the pseudogap opening. We will return to discuss this point in the next section, but concentrate first on the high-temperatures regime where the OMR is proportional to $\tan^2\Theta_H$.

In order to investigate the relation between the Hall effect and the OMR in more detail we show on Fig. 15(a) the OMR data for the films with $y=0$ and $y=0.025$ as a function of $\tan^2\Theta_H$. Since the Hall angle is affected by strain and the

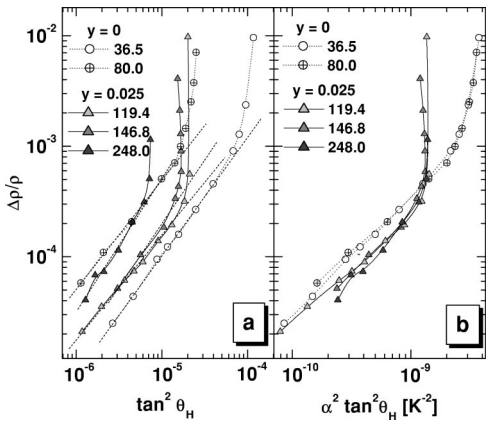

FIG. 15. The OMR as a function of $\tan^2\Theta_H$ (a), and as a function of $\alpha^2\tan^2\Theta_H$ (b). The data include two films with $y=0$ (circles and dotted lines), and three films with $y=0.025$ (triangles and solid lines), with different residual resistivities (in $\mu\Omega$ cm). The dotted and solid lines are guides to the eye. Straight dashed lines are fitted to the data in the high-temperature regions.

OMR is not, the data for specimens with the same y and different ρ_0 fall on separate curves. The high-T region is to the left of the figure, for small values of $\tan\Theta_H$, and small values of the OMR. The dashed straight lines are fitted to the data in this regime. Within experimental error the lines have the same slope, indicating the validity of Eq. (3). As is true for $y=0$ (Fig. 3), the differences between the data for different ρ_0 disappear when we plot the OMR against $\alpha^2\tan^2\Theta_H$ [Fig. 15(b)].

Figure 16 shows the data for all films with positive OMR as a function of $\alpha^2\tan^2\Theta_H$. We see that the high-temperature data follow a set of parallel lines for all specimens, even the nonsuperconducting ones. This shows that in this region the OMR and $\tan^2\Theta_H$ have the same temperature dependence. The straight lines shift downwards as y increases, showing that the coefficient of proportionality decreases as y increases.

We now rewrite Eq. (3) as

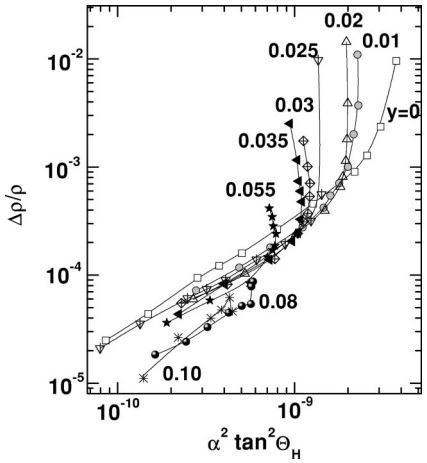

FIG. 16. The OMR as a function of $\alpha^2\tan^2\Theta_H$ for a series of films with various values of y. The high-temperature data are on the left side of the figure. All lines are guides to the eye.

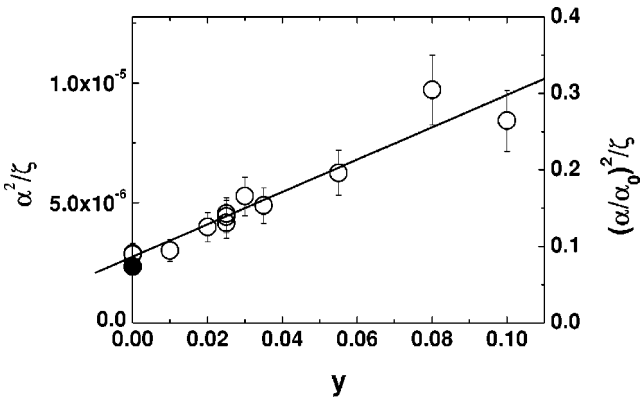

FIG. 17. The dependence of the reciprocal of the parameter ζ/α^2 on y. The scale on the right shows the values of the reciprocal of $\zeta(\alpha_0/\alpha)^2$. The full point is for the $La_{1.83}Sr_{0.17}CuO_4$ single crystal of Harris *et al.*, Ref. 8.

$$\Delta\rho/\rho=(\zeta/\alpha^2)(\alpha^2\tan^2\Theta_H). \tag{7}$$

Since $\alpha^2\tan^2\Theta_H$ is strain independent, and the experiment shows that this is true also for the OMR, it follows that the coefficient ζ/α^2 is also not affected by strain and depends only on y. Moreover it has a surprisingly simple dependence on y. In Fig. 17 we plot its reciprocal as a function of y. This function is seen to increase linearly with y. Since α is y independent, this graph gives us also the y dependence of ζ. We can write

$$\frac{\zeta}{\alpha^2}=\frac{1}{K_0+K_1y}, \tag{8}$$

where $K_0=(2.75\pm0.16)\times10^{-6}$ K^{-4} and $K_1=(6.54\pm0.55)\times10^{-5}$ K^{-4}.

The last column of Table I shows ζ/α^2 multiplied by α_0^2, where α_0 is the value of α for the film with $y=0$ and with the lowest residual resistivity, $\alpha_0=5.65\times10^{-3}$ K^{-2}, so that it is equal to ζ for $y=0$. It changes from 11.05 in the film with $y=0$ to 3.78 in the film with $y=0.10$. We show the reciprocal of this quantity on the right-hand side of Fig. 17. The value of ζ for the $La_{1.83}Sr_{0.17}CuO_4$ single crystal of Ref. 7 is 13.6, in good agreement with the film value.

The coefficient ζ in LSCO is substantially larger then in other high-T_c compounds. In YBCO ζ is equal to 1.5−1.7,[7] and in optimally doped and overdoped $Tl_2Ba_2CuO_{6+\delta}$ it is equal to 3.6 and 2.0, respectively.[18] Since the magnitude of the cotangent does not differ significantly between the different compounds, the ratio seems to depend mainly on the magnitude of the OMR, which reflects the deviation of the Fermi surface from sphericity. The larger ζ in LSCO would than be a natural consequence of the fact that the Fermi surface is more flat in LSCO than in any of the other high-T_c compounds. The addition of impurities reduces ζ to a value comparable to that of the thallium compounds.[18] This is probably a consequence of the reduction of the anisotropy caused by the addition of isotropic impurity scattering. Since the magnetoresistance is an effect of higher order in magnetic field than the Hall effect, it should be more sensitive to the reduction of anisotropy than the Hall angle, leading to a decrease of ζ with y.

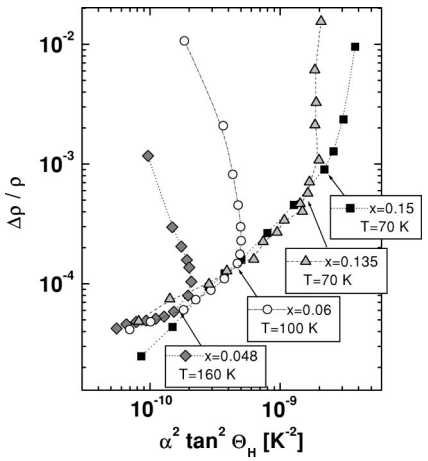

FIG. 18. The OMR as a function of $\alpha^2\tan^2\Theta_H$ for $La_{2-x}Sr_xCuO_4$ films with various amounts of strontium x as indicated in the figure. The dotted lines are guides to the eye. The arrows identify the onsets of the saturation of $\tan\Theta_H$, at the temperatures indicated next to each curve.

D. Pseudogap

We now return to the discussion of the inflection point, and its relation to the pseudogap. The inflection point marks a crossover from the high-T regime, where the OMR is proportional to $\tan^2\Theta_H$, to low-T regime, where this proportionality does not hold. The inflection point is very easy to identify from Fig. 16, even in the case of nonsuperconducting specimens. It is at about 60 to 70 K, regardless of y. This is very different from its shift in underdoped LSCO,[19] which we show on Fig. 18. Here the region where the data follow straight lines moves gradually to higher temperatures, and the slope of the line changes, showing that Eq. (3) is not followed. This is consistent with our previous finding that the T dependence of the OMR loses its S shape in underdoped LSCO because the inflection point moves to temperatures outside the range of the measurements.[19]

When the loss of proportionality between the OMR and $\tan^2\Theta_H$ was first discovered, it was attributed to superconducting fluctuations, which would enhance the OMR in the vicinity of T_c.[7,17] A careful examination of Figs. 16 and 18 shows, however, that the deviation of the two quantities is related to the suppression of $\tan\Theta_H$ rather than to an enhancement of the OMR. This is most easily seen in the specimens with low T_c and in nonsuperconducting specimens, in which the superconductivity does not get in the way. The OMR continues to grow steadily at low temperatures, while $\tan\Theta_H$ first saturates, and then decreases. The temperature of the onset of saturation does not follow the decrease of T_c, but remains constant at about 60 to 70 K in the specimens with zinc, and increases in the underdoped samples, as shown by arrows in Fig. 18. The only specimen in which the enhancement of the OMR may play a role is the one with the

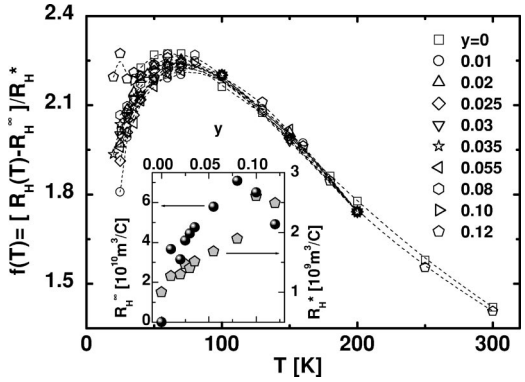

FIG. 19. The rescaled Hall coefficient $[R_H(T)-R_H^{\infty}]/R_H^*$, as a function of temperature. The inset shows the behavior of the parameters R_H^{∞} and R_H^* as a function of y.

optimal T_c, presumably as a result of the close vicinity of the transition to the superconducting state.

A second effect seen on Fig. 14 is a gradual decrease of the OMR, below about 30 K in the film with $y=0.08$, and below about 55 K in the film with $y=0.1$. This effect is y dependent and quite distinct from the y-independent suppression of $\tan\Theta_H$. As we mentioned before, it may be linked to localization effects which eventually lead to a negative OMR in the film with $y=0.12$. We conclude that in the films with zinc there are two distinct anomalies. One, at higher T, is the suppression of $\tan\Theta_H$, while the OMR continues to increase as T is lowered. The second effect, at lower T, is a suppression of the OMR, associated with localization effects.

The suppression of $\tan\Theta_H$ at low T has been observed before in underdoped YBCO (Refs. 53 and 54) and in single-layer and bilayer bismuth compounds[15] suggesting that they may be related to the pseudogap opening. In Ref. 52 it was noted that the suppression of $\tan\Theta_H$ and the broad maximum in R_H both occur at approximately the same temperature as the anomaly in the ^{63}Cu NMR relaxation rate. In the Bi-2212 phase, on the other hand, the tangent anomaly occurs at lower T than the anomalies in the NMR relaxation rate.[15]

The correlation between the maximum in R_H and the suppression of $\tan\Theta_H$ in LSCO may be observed directly from the T dependence of these quantities, which we now examine in more detail. We have rescaled the Hall coefficient R_H by the procedure outlined in Ref. 16, where it is shown that $R_H(T)$ for various values of x collapses to a single curve if plotted as $[R_H(t)-R_H^{\infty}]/R_H^*$, versus $t=T/T^*$. Here R_H^{∞} is the asymptotic value of R_H at high T, while R_H^* and T^* rescale the Hall coefficient and the temperature, respectively. T^*, which identifies the temperature above which the Hall coefficient becomes T independent, was found to decrease from about 700 K for $x=0.1$ to 100 K in the overdoped regime, and was proposed later to be related to the opening of the pseudogap.[20] We apply the same procedure to the data of Fig. 9 for a series of films with zinc, and show the result on Fig. 19. The parameters of the rescaled Hall coefficient are shown in the inset. We find that it is not necessary to rescale the temperature, as could be anticipated from the fact that the

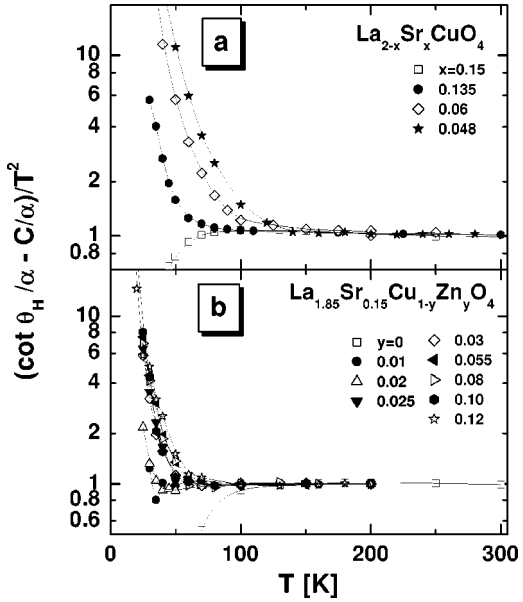

FIG. 20. The rescaled cotangent of the Hall angle, $(\cot\theta_H/\alpha - C/\alpha)/T^2$, as a function of temperature, for several underdoped LSCO films (a), and for a series of films with zinc (b).

maximum in $R_H(T)$ does not shift with y. Comparison with Ref. 16 leads to $T^*\sim 600$ K, independent of y, and close to the result of Ref. 16.

In order to examine the deviation from Eqs. (2) and (5), we show on Fig. 20 the quantity $(\cot\Theta_H/\alpha - C/\alpha)/T^2$. The top panel shows the data for several underdoped LSCO specimens, while the bottom contains the data for the films with zinc. The data for the optimally doped LSCO specimens deviate downwards in both figures, as a result of the close vicinity of T_c. On the other hand, the data for both underdoped LSCO, and LSCZNO, deviate upwards, because of the suppression of $\tan\Theta_H$. The point of deviation clearly shifts to higher T with the decrease of x, but remains constant, at about 50 to 70 K when y changes.

To determine the origin of the suppression of $\tan\Theta_H$ we have analyzed the T dependence of the longitudinal and the Hall conductivities. We find that in the LSCO films both conductivities decrease at low temperatures, unlike the situation in 60 K YBCO,[53] where the suppression was found to be present only in the Hall conductivity. This behavior is illustrated in Fig. 21, were we show the relative change of conductivities for two underdoped, and two films with zinc, normalized to $T=100$ K. The onset of superconductivity is evident at the lowest temperature in the film with $x=0.135$. Apart from this all data display broad maxima in the conductivities, which shift to higher temperatures with decreasing x, and remain constant when y changes, as for the anomalies in $\tan\Theta_H$. However, in each specimen the Hall conductivity displays more pronounced anomalies, and at slightly higher temperatures than the longitudinal conductivity. This pattern indicates that the relatively stronger changes of the Hall conductivity are the cause for the tangent suppression. If we link this effect to the development of the normal-state gap, our analysis reveals two significant results. First, we conclude that the pseudogap opening affects the

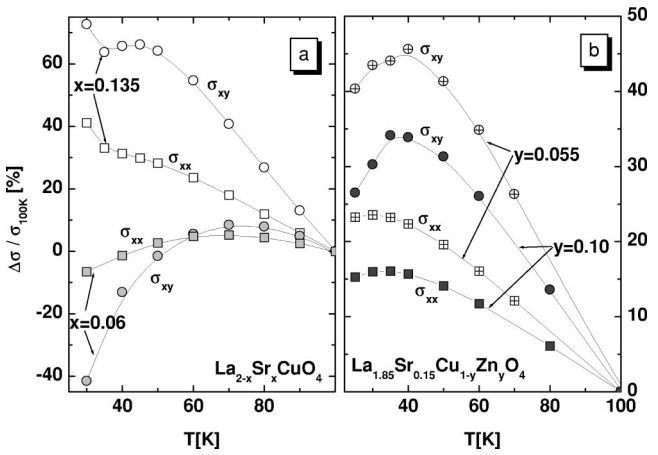

FIG. 21. The relative change of the longitudinal and Hall conductivities, normalized at $T=100$ K. The data are for two underdoped LSCO films with $x=0.135$ and $x=0.06$ (a), and for two films with $y=0.055$, and $y=0.06$ (b). The Hall conductivity is measured at 8 tesla. All lines are guides to the eye.

Hall conductivity more effectively than the longitudinal conductivity. Secondly, the pattern of the evolution with x and y indicates that the temperature at which the pseudogap opens is not affected by the zinc doping, while it shifts to higher temperatures for underdoped specimens.

Finally, we would like to comment on the decrease of the OMR at low temperatures, which we propose to link to the localization effects. These are not the usual effects of weak localization observed in conventional disordered metals. We have made a careful study of the behavior of the magnetoresistance of the zinc-doped and the underdoped LSCO at temperatures below those discussed in the present paper, at $T<25$ K. A detailed account will be published separately.[51] The results show that weak localization effects are absent. Instead, we find strong evidence of the influence of spin-disorder scattering on the transport properties. This is not surprising. In LSCO the carriers move in the disordered magnetic background of the CuO_2 planes, and themselves influence the type of this disorder, contributing to the T dependence of the resistivity. There is plenty of evidence that the localization of carriers is nonuniform in LSCO,[52,55–57] possibly in the form of stripes.[58] It is important to point out that these localization effects appear to be distinctly different from the effects of the normal-state pseudogap opening which are observed in the high-temperature range.

V. DISCUSSION

A. Normal-state transport parameters: the effects of impurities and strain

The main subject of this study, which is the influence of impurities and strain on the normal-state transport properties, may be summarized as follows.

(1) *Strain.* If we exclude the effect of grain-boundary scattering, the strain affects ρ_0, A, α, and C in approximately the same way. A decrease of the c-axis lattice parameter, accompanied by an increase of the a-axis parameter (i.e., tensile in-plane strain), results in an increase of all transport parameters, with a fractional changes of about 100% per 0.01 Å. The OMR, on the other hand, is not affected by strain.

(2) *Impurities.* The addition of zinc does not change the carrier concentration. It adds an impurity scattering term to the residual resistivity and to the elastic Hall scattering term. It has almost no effect on A and does not affect α. These results are consistent with previous observations. However, the OMR is more strongly suppressed by impurities than $\tan^2\Theta_H$, so that ζ decreases with an increase of impurities.

Before we compare these results to more sophisticated theoretical models, we compare them first to a simple Drude model, where the resistivity is given by $\rho=m^*/ne^2\tau$, where n is the carrier concentration, m^* the effective mass, and τ^{-1} the relaxation rate, with both an elastic and an inelastic part. The Hall effect and the magnetoresistance are described by the relations $\cot\Theta_H \sim (\omega_c\tau)^{-1}$ and $\Delta\rho/\rho \propto (\omega_c\tau)^2$, where $\omega_c = eB/m^*$ is the cyclotron frequency. In our experiment the tensile strain, which increases the in-plane distances, causes simultaneous proportional increases in all transport coefficients, i.e., it changes both the elastic and inelastic terms in ρ and $\cot\Theta_H$ in the same way. In the Drude model this can only be explained by an increase of the effective mass, which would qualitatively be a reasonable outcome of the increase of the in-plane lattice distances. However, we would expect the OMR to change as well, since it is proportional to ω_c^2, and this is not observed. In addition, ζ depends on the impurity content, while it should be constant in this model.

We now consider more complicated approaches, designed to reproduce the different T dependences of ρ and $\cot\Theta_H$. We start with the non-FL models. The original model by Anderson[28] invokes a picture of holons and spinons which separately control the longitudinal and transverse relaxation rates, respectively. A subsequent model, also with two distinct relaxation rates, assumes that the electronic scattering in cuprates is sensitive to the charge-conjugation symmetry of quasiparticles.[29] The main feature of both models is that two relaxation rates, which are a result of spin-charge separation or different parity of the quasiparticle states, exist at each point of the Fermi surface. Since in these models the Hall effect and magnetoresistance are governed by the same relaxation rate, their ratio should behave as in the Drude model, i.e., the coefficient ζ should be independent of temperature, impurities, or strain. Our results are inconsistent with these expectations.

The FL models assume the existence of quasiparticles with strongly anisotropic scattering rates along the Fermi surface. Various anisotropies have been proposed, including ''hot spots'' and ''cold spots,'' small regions of the Fermi surface in which the scattering is either much stronger, or much weaker, respectively, than in the remaining parts, and has a distinctly different T dependence.[9,11,22–24,26,27] Possible microscopic origins of different scattering rates include antiferromagnetic spin fluctuations, charge fluctuations, and pairing fluctuations which may couple preferentially to carriers with certain momenta.[22,24,25] These concepts are based on ARPES results which indicate that single particle scattering is much stronger along the $(0,0)$-$(\pi,0)$ and $(0,0)$-$(0,\pi)$ directions than along the zone diagonals.[59] Since ρ and $\cot\Theta_H$

involve scattering in different regions of the Fermi surface, it is then possible to reproduce the different T dependences of ρ and $\cot\Theta_H$.

The magnetoresistance has been evaluated in only two of these models.[24,27] One of them is the cold-spots model of Ioffe and Millis,[24] which assumes that the in-plane resistivity is controlled by carriers with momenta along the zone diagonals, which have an FL scattering rate proportional to T^2 (cold spots). In the regions away from the diagonal, the scattering rate makes a large T-independent but momentum-dependent contribution. The linear T dependence of the resistivity results from the linear T dependence of the width of the cold region. This model has been used sucsessfully to explain several experiments.[60,61] However, the magnitude of the OMR is much larger than experimentally observed and the coefficient ζ is found to be T dependent. These features disagree with both the previous experiments, and with the present study. The model predicts a violation of Matthiessen's rule and this is also contrary to the experimental data. In addition, the ratio ζ should increase with y, while our experiment indicates a decrease.

A second calculation of the OMR is based on the phenomenological additive two-τ model, which assumes two distinct relaxation rates τ_1 and τ_2.[26,27] The Fermi surface is assumed to have large flat regions around M points with a short relaxation time $\tau_1 \sim T^{-1}$ and large Fermi velocity (hot spots). The sharp corners around the nodal points have a long relaxation time $\tau_2 \sim T^{-2}$ and small Fermi velocity (cold spots). The carriers from the hot spots dominate the in-plane resistivity, while cold regions dominate the Hall conductivity, leading to T dependences which agree with experiment. This model leads to an almost T-independent ratio ζ, close to the experimental results. The impurity effects on ζ have not been evaluated. ARPES experiments on bismuth compounds do not confirm the assumed character of the Fermi surface.[62] The flat portion around the M points is observed to be smaller, and the velocities in the hot region are smaller than in the cold region. Interestingly, the large flat portions around M may better approximate the real Fermi surface observed in LSCO.

Apart from these comparisons the effect of strain creates a stringent test of the FL models. The models have to reflect the fact that strain affects all transport coefficients similarly, but does not affect the OMR. The effect of strain on the Fermi surface can change the relative size of the cold and hot areas. In the two-τ model the ratio of the contributions from the cold and hot areas appears to be approximately the same for the Hall conductivity and for the magnetoresistance, so that the different effects of strain on these quantities may be difficult to reproduce. However, a detailed comparison is needed to evaluate this effect.

A recent ARPES study provides more detail on the properties of the Fermi surface.[33] It finds that in $Bi_2Sr_2CaCu_2O_{8+\delta}$ (Bi2212) the single-particle scattering rate contains a large T-independent part which disappears only in the vicinity of the nodal directions, plus a part linearly dependent on temperature and energy which extends over most of the Fermi surface and becomes almost T independent in the vicinity of the $(\pi,0)$ and $(0,\pi)$ directions. This result motivated the development of two new theoretical approaches.[31,32]

The model of Varma and Abrahams combines the predictions of the marginal FL hypothesis for the inelastic scattering linear in T with an elastic, strongly anisotropic term, which results from small-angle forward scattering by impurities situated away from the CuO_2 planes.[31] The forward scattering produces new contributions to $\tan\Theta_H$ so that instead of Eq. (2) the resistivity should be proportional to $\sqrt{\cot\Theta_H}$. The data for impurity-doped single crystals of YBCO support this form.[31] A preliminary analysis of our data shows that this proportionality is followed for a film with $y=0$ and small strain. However, deviations appear with larger strain and at this point it is not clear to us how to incorporate the strain into the model.

Another model introduced recently is the two-patch model, designed to analyze the normal-state transport properties of cuprates using the Boltzmann equation.[32] The Brillouin zone and the Fermi surface are divided into regions where the scattering between the electrons is strong and the Fermi velocity is low (hot patches), and regions where the scattering is weak and the Fermi velocity is large (cold patches). For Bi-based cuprates the hot patches are centered around the saddle (M) points of the Brillouin zone, while the cold patches are centered around the nodal points, along the $\Gamma Y(X)$ direction of the Brillouin zone. Three distinct temperature dependences for the scattering amplitude are assumed, T^2 in the cold region, T for the interpatch (hot-cold) scattering, and a T-independent value in the hot region. The resulting scattering amplitude $1/\tau_k$ obtained from the scattering matrix is strongly momentum dependent. The low-temperature behavior, in contrast with other similar approaches,[23,24,26,27] is always non-FL, with a linear T dependence in the cold patches and a constant in the hot patches, as observed by the ARPES spectra.[33] This model gives a reasonable description of the transport properties of the Bi-based cuprates. When comparing it to our experiment we note first that the model predicts an increase of the residual resistivity and of the constant term in the cotangent when the size of hot regions increases. Since hot regions may be expected to be larger in the flatter Fermi surface of LSCO, this would explain why the residual resistivities and the constant term in the cotangent are larger in LSCO than in other cuprates. In addition, the T dependence of the longitudinal and the Hall conductivities in this model are both controlled primarily by the density of states and the Fermi velocities in the cold regions. The similar effect of strain on these quantities could then be explained by the effect of strain on the cold-region properties. It is not clear if this model can reproduce the insensitivity of the OMR to strain. To see this, more detailed calculations using the LSCO Fermi surface would be necessary.

To summarize this part of the discussion, we conclude that our results disagree with most of the earlier theoretical models. New theoretical models,[31,32] which include the Fermi surface properties in a more realistic way may turn out to be more compatible with the experiments. More detailed

comparisons are needed to evaluate these new proposals, including the effects of strain, as described in this study.

B. Pseudogap: the effect of impurities and underdoping

Next we comment on the markedly different effect of a change of x (in underdoped LSCO) and y (in zinc-doped LSCO) on the pseudogap, as inferred from the suppression of $\tan\Theta_H$. The gradual opening of a pseudogap was originally suggested to explain anomalies in the behavior of various normal-state properties.[21] These anomalies take the form of a crossover temperature between two different T dependences. An example is the Hall effect anomaly, where below the crossover temperature T^* the Hall coefficient is T dependent.[16] The crossover temperatures for different properties and materials differ a great deal. However, most of them increase with underdoping. For example, in LSCO T^* increases from 100 to 700 K when x is decreased from 0.3 to 0.05.[16]

ARPES studies provide a number of important insights into pseudogap phenomena. The opening of the gap in the normal-state excitation spectrum above T_c has been detected in underdoped Bi2212 and Bi2201. Its momentum dependence is consistent with d-wave symmetry, and as the temperature decreases, the normal-state gap evolves smoothly into a superconducting gap.[63–68] The temperatures of the pseudogap opening from tunneling, optical conductivity, and Raman scattering experiments are in quite good agreement with the ARPES data on Bi2212.[21]

The situation is more confusing for LSCO. The photoemission studies are more difficult because of quick surface degradation at high temperatures. The ARPES studies were limited to low temperatures,[56,57] while angle-integrated photoemission spectra (AIPES) were investigated as a function of T.[69] An AIPES study of optimally doped LSCO reveals a suppression of the density of states near the Fermi energy as T is lowered, extending to about 30–35 meV.[69] This energy corresponds to about 350 to 400 K, which is somewhat lower than the Hall-effect crossover temperature T^* in optimally doped LSCO.[16] However, no evidence was found of the connection between this pseudogap and the superconducting gap. The ARPES study focuses on the dependence on x of the spectra measured around the saddle point $(\pi,0)$ and concludes that the energy gap Δ increases smoothly with decreasing x. In an optimally doped crystal Δ is a superconducting gap of about 8 meV, while in an underdoped specimen with $x=0.05$ it is a normal-state gap of about 25 meV.[56,57] In addition, the spectral weight around the nodal points becomes severely depleted below $x=0.12$, while the band around the saddle points is very flat.

In order to correlate the suppression of $\tan\Theta_H$, observed in our measurements, with the other anomalies, we compare their x dependences on Fig. 22. The full circles show the temperature $T_{\tan}$ at which $\tan\Theta_H$ is suppressed for the underdoped LSCO films from Fig. 18. As we discussed earlier, in optimally doped films the vicinity of the superconducting state prevents the suppression of $\tan\Theta_H$ from being seen. Instead we plot the temperature of the inflection point for $x=0.15$ and $x=0.225$. We also plot T_c for all films. Comparing the two dependences we see that the line describing the suppression of $\tan\Theta_H$ is considerably higher than the T_c line in the underdoped films, but approaches T_c in the optimally doped films.

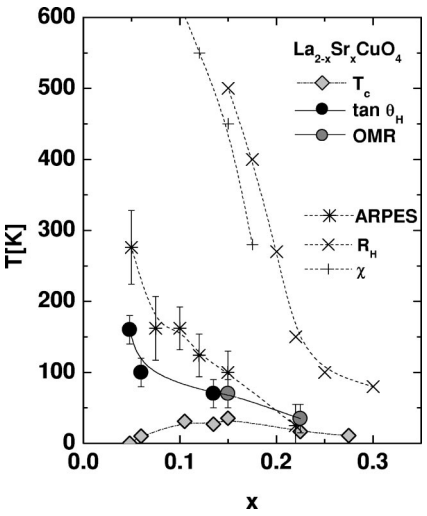

FIG. 22. The x dependence of several quantities for $La_{2-x}Sr_xCuO_4$. Circles: temperature of the tangent suppression (black), inflection points from OMR data (grey); diamonds: T_c; stars: Δ from ARPES, Ref. 56; crosses: anomalies from Hall effect and susceptibility, Ref. 16. All lines are guides to the eye.

Next we include the crossover temperatures of the Hall effect (T^*), and the susceptibility from Ref. 16, and the gap from the ARPES experiments.[57] Our results for T^* give a value of about 600 K, which is in reasonable agreement with the T^* line in the figure. It is clear that $T_{\tan}$ is considerably smaller than T^*. Instead, it seems to be quite closely related to the normal-state gap value inferred from the ARPES experiments. Therefore we conclude that the Hall conductivity in the underdoped films is strongly affected by the opening of the normal−state gap around the saddle point $(\pi,0)$.

It is important to point out here that this conclusion does not necessarily mean that the nodal excitations are unimportant for the normal-state Hall effect. As we discussed, in the underdoped specimens Eq. (3), characteristic for the normal state of the optimally doped films, is not followed. This indicates that in the underdoped samples the density of states which contributes to the transport properties is already severely affected at high temperatures, and this is reflected in the shift of T^* with underdoping. While this effect may be a precursor of the normal-state gap opening, the ARPES results suggest that there is another possibility, related to the decrease of the spectral weight around nodal points in the underdoped specimens.[56,57] It is entirely possible that in the optimally doped range the nodal density of states contributes decisively to the transport properties, and after it is eliminated by the underdoping, the only contribution which is left is from the saddle point. Alternatively, the effect may be related to the shrinking of the size of Fermi surface regions without a gap around the nodal points. This would be more in accord with the fact that a similar coincidence between $T_{\tan}$ and the normal-state gap opening deduced from ARPES occurs for bismuth compounds,[15,63] in which there is no sub-

stantial decrease of the spectral weight around nodal points in the underdoped compositions. This would indicate that the origin of the effect of normal-state gap opening on the suppression of $\tan\Theta_H$ is the same for different cuprate compounds.

Finally we discuss the effect of zinc on the pseudogap. Our experiment shows that both crossover temperatures T^* and $T_{\tan}$ remain constant when y changes, indicating that the opening of the normal-state gap is unaffected by the zinc. On the other hand, the magnitudes of both the OMR and $\tan\Theta_H$ decrease with y, with the OMR affected more strongly, as shown by Eq. (8). These two seemingly contrasting results, i.e., the constant temperature of the gap opening, and the influence of impurities on the transport properties, may be reconciled if one assumes that the effect of impurities on the pseudogap is confined to the immediate area surrounding the impurity, while away from them the pseudogap remains intact. In fact, there have been many suggestions that this is indeed the case. ^{63}Cu NMR experiments on Zn-doped YBCO find an enhancement of the antiferromagnatic correlations around Zn impurities, while the crossover temperature in the relaxation rate remains constant.[52] Similar conclusions have been inferred from neutron scattering experiments,[70] from ^{89}Y NMR measurements,[71] and ESR measured on gadolinium sites in Gd- and Zn-doped YBCO.[72] A local effect of zinc impurities on the pseudogap has also been suggested by studies of thermopower[73] and specific heat in YBCO.[74]

These local effects resemble the ''swiss cheese'' model,[75] in which charge carriers around each Zn impurity are excluded from superconductivity. However, the real effect of impurities on the normal state properties is more complex. While the temperature of the pseudogap opening is unaffected in the main volume of the sample, the other properties are strongly affected. These effects are very different from those in underdoped LSCO, as can be seen from the fact that the main features of the normal state, given by Eqs. (1) to (3), survive in the films with zinc.

VI. CONCLUSIONS

The analysis of the structure and microstructure of the $La_{1.85}Sr_{0.15}Cu_{1-y}Zn_yO_4$ films shows that they grow with variable amounts of built-in strain resulting from the partial relief of the lattice mismatch by dislocations. Both compressive and tensile in-plane strain with respect to the bulk lattice parameters are observed. They are accompanied by expansion or compression of the c-axis lattice parameter, respectively. Weak links appear in some films, but they have no influence on the normal-state transport. In some other films the grain-boundary scattering enhances the residual resistivity but does not affect the remaining transport parameters.

Strain affects the superconducting and the normal-state transport properties. T_c decreases with the decrease of the $c-$axis lattice parameter at a rate of about 670 K/Å. The decrease of T_c is accompanied by a linear increase of ρ_0, A, α, and C at a rate of about 15% per K. The addition of zinc adds an impurity scattering term to ρ_0, and to C, the constant term in $\cot\Theta_H$, while the slope of the T dependence of the resistivity and the slope of the T^2 dependence of the cotangent remain unchanged. The effects of impurities and strain on ρ_0 are additive, while they are multiplicative in the case of C. The OMR is independent of strain. Over a limited T range, above the inflection point, the OMR is proportional to $\tan^2\Theta_H$. The coefficient of proportionality ζ depends on strain and on the impurities, showing that the relaxation rate which governs the Hall effect is not the same as that of the magnetoresistance. A comparison of these results with the available theoretical models of the normal state indicates that none of them can fully describe the experiments. New models which take the properties of the Fermi surface into account more realistically may be compatible, but a more detailed evaluation, including the strain effects which we observe will be necessary.

In addition, we observe a suppression of $\tan\Theta_H$ for underdoped and zinc-doped films, and show that it can be associated with the opening of a gap in the normal-state excitation spectrum. The temperature of the pseudogap opening does not change with the addition of zinc impurities but it increases when the Sr-La ratio is decreased. At temperatures lower than the temperature of the pseudogap opening, the OMR decreases as a result of localization effects.

ACKNOWLEDGMENTS

We would like to thank M. Gershenson and S-W. Cheong for their cooperation and sharing of laboratory facilities. We also thank T. E. Madey for providing the facilities for the AFM study and for helping with its interpretation, and C. L. Chien for the four-cycle X-ray diffractometer measurements. We appreciate the discussions with Elihu Abrahams, Piers Coleman, Gabriel Kotliar, and Andrew Millis. We also take the opportunity to thank Richard Newrock and the Physics Department of the University of Cincinnati for help with the construction of the target chamber. This work was supported by the Polish Committee for Scientific Research, KBN, under Grants No. 2 P03B 09414 and 7 T08A 00520, by the Naval Research Laboratory, by the Rutgers Research Council, and by the Eppley Foundation for Research. A. Perali acknowledges partial support from Fondazione ''Angelo della Riccia.''

[1] Y. Iye, in *Physical Properties of High Temperature Superconductors III*, edited by D. M. Ginsburg (World Scientific, Singapore, 1992), p. 285.

[2] M. Gurvitch, and A.T. Fiory, Phys. Rev. Lett. **59**, 1337 (1987).

[3] K. Takagi, B. Batlogg, H.L. Kao, J. Kwo, R.J. Cava, J.J. Krajewski, and W.F. Peck, Phys. Rev. Lett. **69**, 2975 (1992).

[4] S.W. Cheong, S.E. Brown, Z. Fisk, R.S. Kwok, J.D. Thompson, E. Zirngiebl, G. Gruner, D.E. Peterson, G.L. Wells, R.B.

Schwarz, and J.R. Cooper, Phys. Rev. B **36**, 3913 (1987); Z.Z. Wang, J. Clayhold, N.P. Ong, J.M. Tarascon, L.H. Greene, W.R. McKinnon, and G.W. Hull, *ibid.* **36**, 7222 (1987); P. Chaudhari, R.T. Collins, P. Freitas, R.J. Gambino, J.R. Kirtley, R.H. Koch, R.B. Laibowitz, F.K. LeGoues, T.R. McGuire, T. Penney, Z. Schlesinger, A.P. Segmüller, S. Foner, and E.J. McNiff, Jr., *ibid.* **36**, 8903 (1987).

[5] T.R. Chien, Z.Z. Wang, and N.P. Ong, Phys. Rev. Lett. **67**, 2088 (1991).

[6] J. M. Ziman, *Electrons and Phonons, The Theory of Transport Phenomena in Solids* (Oxford University Press, Oxford, 1960), p. 334.

[7] J.M. Harris, Y.F. Yan, P. Matl, N.P. Ong, P.W. Anderson, T. Kimura, and K. Kitazawa, Phys. Rev. Lett. **75**, 1391 (1995).

[8] J.M. Harris, Y.F. Yan, and N.P. Ong, Phys. Rev. B **46**, 14 293 (1992); Peng Xiong, Gang Xiao, and X.D. Wu, *ibid.* **47**, 5516 (1993); B. Bucher, P. Steiner, J. Karpinski, E. Kaldis, and P. Wachter, Phys. Rev. Lett. **70**, 2012 (1993); J.M. Harris, H. Wu, N.P. Ong, R.L. Meng, and C.W. Chu, Phys. Rev. B **50**, 3246 (1994).

[9] A. Carrington, A.P. Mackenzie, C.T. Lin, and J.R. Cooper, Phys. Rev. Lett. **69**, 2855 (1992); A. Carrington, D.J.C. Walker, A.P. Mackenzie, and J.R. Cooper, Phys. Rev. B **48**, 13 051 (1993).

[10] Gang Xiao, Peng Xiong, and Marta Z. Cieplak, Phys. Rev. B **46**, 8687 (1992).

[11] C. Kendziora, D. Mandrus, L. Mihaly, and L. Forro, Phys. Rev. B **46**, 14 297 (1992).

[12] T. Ito, K. Takenaka, and S. Uchida, Phys. Rev. Lett. **70**, 3995 (1993).

[13] B. Wuyts, E. Osquiguil, M. Maenhoudt, S. Libbrecht, Z.X. Gao, and Y. Bruynseraede, Phys. Rev. B **47**, 5512 (1993).

[14] Yoichi Ando and T. Murayama, Phys. Rev. B **60**, R6991 (1999).

[15] Z. Konstantinović, Z.Z. Li, and H. Raffy, Phys. Rev. B **62**, R11 989 (2000).

[16] H.Y. Hwang, B. Batlogg, H. Takagi, H.K. Kao, J. Kwo, R.J. Cava, J.J. Krajewski, and W.F. Peck, Jr., Phys. Rev. Lett. **72**, 2636 (1994).

[17] T. Kimura, S. Miyasaka, H. Takagi, K. Tamasaku, H. Eisaki, S. Uchida, K. Kitazawa, M. Hiroi, M. Sera, and N. Kobayashi, Phys. Rev. B **53**, 8733 (1996).

[18] A.W. Tyler, Y. Ando, F.F. Balakirev, A. Passner, G.S. Boebinger, A.J. Schofield, A.P. Mackenzie, and O. Laborde, Phys. Rev. B **57**, R728 (1998).

[19] F.F. Balakirev, I.E. Trofimov, S. Guha, Marta Z. Cieplak, and P. Lindenfeld, Phys. Rev. B **57**, R8083 (1998).

[20] B. Batlogg, H.Y. Hwang, H. Takagi, R.J. Cava, H.L. Kao, and J. Kwo, Physica C **235-240**, 130 (1994).

[21] For a review see T. Timusk and B. Statt, Rep. Prog. Phys. **62**, 61 (1999).

[22] B.P. Stojković and D. Pines, Phys. Rev. Lett. **76**, 811 (1996).

[23] R. Hlubina and T.M. Rice, Phys. Rev. B **51**, 9253 (1995).

[24] L.B. Ioffe and A.J. Millis, Phys. Rev. B **58**, 11 631 (1998).

[25] S. Caprara, M. Sulpizi, A. Bianconi, C. Di Castro, and M. Grilli, Phys. Rev. B **59**, 14 980 (1999).

[26] A.T. Zheleznyak, V.M. Yakovenko, and H.D. Drew, Phys. Rev. B **57**, 3089 (1998).

[27] A.T. Zheleznyak, V.M. Yakovenko, and H.D. Drew, Phys. Rev. B **59**, 207 (1999).

[28] P.W. Anderson, Phys. Rev. Lett. **67**, 2092 (1991).

[29] P. Coleman, A.J. Schofield, and A.M. Tsvelik, J. Phys.: Condens. Matter **8**, 9985 (1996); Phys. Rev. Lett. **76**, 1324 (1996).

[30] J. Cerne, M. Grayson, D.C. Schmadel, G.S. Jenkins, H.D. Drew, R. Hughes, A. Dabkowski, J.S. Preston, and P.-J. Kung, Phys. Rev. Lett. **84**, 3418 (2000).

[31] C.M. Varma and Elihu Abrahams, Phys. Rev. Lett. **86**, 4652 (2001); **88**, 139903 (2002).

[32] A. Perali, M. Sindel, and G. Kotliar, Eur. Phys. J. B **24**, 487 (2001).

[33] T. Valla, A.V. Fedorov, P.D. Johnson, Q. Li, G.D. Gu, and N. Koshizuka, Phys. Rev. Lett. **85**, 828 (2000).

[34] K. Karpińska, Marta Z. Cieplak, S. Guha, A. Malinowski, T. Skośkiewicz, W. Plesiewicz, M. Berkowski, B. Boyce, T.R. Lemberger, and P. Lindenfeld, Phys. Rev. Lett. **84**, 155 (2000).

[35] H. Sato and M. Naito, Physica C **274**, 221 (1997).

[36] H. Sato, A. Tsukada, M. Naito, and A. Matsuda, Phys. Rev. B **61**, 12 447 (2000).

[37] J.-P. Locquet, J. Perret, J. Fompeyrine, E. Mächler, J.W. Seo, and G. Van Tendeloo, Nature (London) **394**, 453 (1998).

[38] A. Perali and G. Varelogiannis, Phys. Rev. B **61**, 3672 (2000).

[39] Marta Z. Cieplak, A. Malinowski, K. Karpińska, S. Guha, A. Krickser, B. Kim, Q. Wu, C.H. Shang, M. Berkowski, and P. Lindenfeld, Phys. Rev. B **65**, 100504(R) (2002).

[40] M.Z. Cieplak, M. Berkowski, S. Guha, E. Cheng, A.S. Vagelos, D.J. Rabinowitz, B. Wu, I.E. Trofimov, and P. Lindenfeld, Appl. Phys. Lett. **65**, 3383 (1994).

[41] Marta Z. Cieplak, K. Karpińska, J. Domagala, E. Dynowska, M. Berkowski, A. Malinowski, S. Guha, M. Croft, and P. Lindenfeld, Appl. Phys. Lett. **73**, 2823 (1998).

[42] H. Lüth, *Surfaces and Interfaces in Solids* (Springer-Verlag, Berlin, 1993).

[43] *Strained-Layer Superlattices: Materials Science and Technology*, Vol. 33 of *Semiconductors and Semimetals*, edited by T. P. Pearsall (Academic Press, Boston, 1991).

[44] Marta Z. Cieplak, S. Guha, Q. Wu, B. Kim, M. Berkowski, and C. H. Shang (unpublished).

[45] A.A. Gapud, J.R. Liu, J.Z. Wu, W.N. Kang, B.W. Kang, S.H. Yun, and W.K. Chu, Phys. Rev. B **56**, 862 (1997); C. Quitmann, P. Almeras, J. Ma, R.J. Kelley, H. Berger, C. Xueyu, G. Margaritondo, and M. Onellion, *ibid.* **53**, 6819 (1996).

[46] Y. Fukuzumi, K. Mizuhashi, K. Takenaka, and S. Uchida, Phys. Rev. Lett. **76**, 684 (1996).

[47] F. Gugenberger, Ch. Meingast, G. Roth, K. Grube, V. Breit, T. Weber, H. Wühl, S. Uchida, and Y. Nakamura, Phys. Rev. B **49**, 13 137 (1994).

[48] R. Gross, in *Interfaces in High-T_c Superconducting Systems*, edited by S. L. Shindé and D. A. Rudman (Springer-Verlag, New York, 1994), p. 176.

[49] Marta Z. Cieplak, S. Guha, H. Kojima, P. Lindenfeld, Gang Xiao, J.Q. Xiao, and C.L. Chien, Phys. Rev. B **46**, 5536 (1992).

[50] A.A. Abrikosov and L.P. Gor'kov, Sov. Phys. JETP **12**, 1243 (1961).

[51] A. Malinowski, Marta Z. Cieplak, K. Karpinska, W. Plesiewicz, T. Skoskiewicz, M. Berkowski, S. Guha, and P. Lindenfeld (unpublished).

[52] M.-H. Julien, T. Fehér, M. Horcatić, C. Berthier, O.N. Bakharev, P. Ségransan, G. Collin, and J.-F. Marucco, Phys. Rev. Lett. **84**, 3422 (2000).

[53] Z.A. Xu, Y. Zhang, and N.P. Ong, cond-mat/9903123 (unpublished).
[54] Y. Abe, K. Segawa, and Y. Ando, Phys. Rev. B **60**, R15 055 (1999).
[55] M.-H. Julien, F. Borsa, P. Caretta, M. Horcatić, C. Berthier, and C.T. Lin, Phys. Rev. Lett. **83**, 604 (1999).
[56] A. Ino, C. Kim, M. Nakamura, T. Yoshida, T. Mizokawa, Z.-X. Shen, A. Fujimori, T. Kakeshita, H. Eisaki, and S. Uchida, Phys. Rev. B **62**, 4137 (2000).
[57] A. Ino, C. Kim, M. Nakamura, T. Yoshida, T. Mizokawa, Z.-X. Shen, A. Fujimori, T. Kakeshita, H. Eisaki, and S. Uchida, Phys. Rev. B **65**, 094504 (2002).
[58] V.J. Emery, S.A. Kivelson, and O. Zachar, Phys. Rev. B **56**, 6120 (1997); S.A. Kivelson, E. Fradkin, and V.J. Emery, Nature (London) **393**, 550 (1998); J. Zaanen and M. Oleś, Ann. Phys. (Leipzig) **5**, 224 (1996); M. Fleck, A.I. Lichtenstein, E. Pavarini, and A.M. Oleś, Phys. Rev. Lett. **84**, 4962 (2000).
[59] Z.X. Shen and D. Dessau, Phys. Rep. **253**, 1 (1995).
[60] D. van der Marel, Phys. Rev. B **60**, R765 (1999).
[61] T. Xiang and W.N. Hardy, Phys. Rev. B **63**, 024506 (2001).
[62] J.C. Campuzano, H. Ding, M.R. Norman, M. Randeria, A.F. Bellman, T. Yokoya, T. Takahashi, H. Katayama-Yoshida, T. Mochiku, and K. Kadowaki, Phys. Rev. B **53**, R14 737 (1996).
[63] H. Ding, T. Yokaya, T. Campuzano, T. Takahasi, M. Randeria, M.R. Norman, T. Mochiku, K. Kadowaki, and J. Giapinzakis, Nature (London) **382**, 2628 (1996).
[64] A.G. Loeser, Z.-X. Shen, D.S. Dessau, D.S. Marshall, C.H. Park, P. Fournier, and A. Kapitulnik, Science **273**, 325 (1996).
[65] J.M. Harris, Z.-X. Shen, P.J. White, D.S. Marshall, M.C. Schabel, J.N. Eckstein, and I. Bozovic, Phys. Rev. B **54**, R15 665 (1996).
[66] P.J. White, Z.-X. Shen, C. Kim, J.M. Harris, A.G. Loeser, P. Fournier, and A. Kapitulnik, Phys. Rev. B **54**, R15 669 (1996).
[67] M.R. Norman, H. Ding, M. Randeria, J.C. Campuzano, T. Yokoya, T. Takeuchi, T. Takahashi, T. Mochiku, K. Kadowaki, P. Guptasarma, and D.G. Hinks, Nature (London) **392**, 157 (1998).
[68] F. Ronning, C. Kim, D.L. Feng, D.S. Marshall, A.G. Loeser, L.L. Miller, J.N. Eckstein, I. Bozovic, and Z.-X. Shen, Science **282**, 2067 (1998).
[69] T. Sato, T. Yokoya, Y. Naitoh, T. Takahashi, K. Yamada, and Y. Endoh, Phys. Rev. Lett. **83**, 2254 (1999).
[70] K. Kakurai, S. Shamoto, T. Kiyokura, M. Sato, J.M. Tranquada, and G. Shirane, Phys. Rev. B **48**, 3485 (1993); Y. Sidis, P. Bourges, B. Hennion, L.P. Regnault, R. Villeneuve, G. Collin, and J.F. Marucco, *ibid.* **53**, 6811 (1996); H.F. Fong, P. Bourges, Y. Sidis, L.P. Regnault, J. Bossy, A. Ivanov, D.L. Milius, I.A. Aksay, and B. Keimer, Phys. Rev. Lett. **82**, 1939 (1999).
[71] A.V. Mahajan, H. Alloul, G. Collin, and J.F. Marucco, Phys. Rev. Lett. **72**, 3100 (1994).
[72] A. Jánossy, J.R. Cooper, L.-C. Brunel, and A. Carrington, Phys. Rev. B **50**, 3442 (1994).
[73] J.L. Tallon, J.R. Cooper, P.S.I.P.N. de Silva, G.V.M. Williams, and J.W. Loram, Phys. Rev. Lett. **75**, 4114 (1995).
[74] J.W. Loram, K.A. Mirza, J.W. Wade, J.R. Cooper, and W.Y. Liang, Physica C **235-240**, 134 (1994).
[75] B. Nachumi, A. Keren, K. Kojima, M. Larkin, G.M. Luke, J. Merrin, O. Tchernyshov, Y.J. Uemura, N. Ichikawa, M. Goto, and S. Uchida, Phys. Rev. Lett. **77**, 5421 (1996).